Journal of Catalysis 393 (2021) 259–280

Contents lists available at ScienceDirect

Journal of Catalysis

journal homepage: www.elsevier.com/locate/jcat

Mini-review

Characterisation and reactivity of oxygen species at the surface of metal oxides

M. Anpo [a,b], G. Costentin [c], E. Giamello [d], H. Lauron-Pernot [c,*,1], Z. Sojka [e]

[a] Department of Applied Chemistry, Osaka Prefecture University Sakai, Osaka 599-8531, Japan
[b] State Key Laboratory of Photocatalysis on Energy and Environment, Fuzhou University, Fuzhou, Fujian 350002, PR China
[c] Sorbonne Université, CNRS, Laboratoire de Réactivité de Surface, LRS, F-75005 Paris, France
[d] Dipartimento di Chimica, Via Giuria 7, 10125 Torino, Italy
[e] Faculty of Chemistry, Jagiellonian University, ul. Gronostajowa 2, 30-387 Kraków, Poland

ARTICLE INFO

Article history:
Received 9 July 2020
Revised 30 September 2020
Accepted 8 October 2020
Available online 22 October 2020

Keywords:
Oxygen species
EPR
Photoluminescence spectroscopy
Basicity

ABSTRACT

Surface reactive oxygen species play a fundamental role in selective oxidation and combustion reactions catalyzed by metal oxides. Unravelling the nature of these transient species, and understanding the details of both their electronic structure and reactivity has been for decades one of the prime research areas of surface and catalytic chemistry. The longstanding activity of Michel Che in this area has been a source of inspiration for generation of researchers, and constitute his outstanding and enduring scientific legacy. Present review provides a survey of the surface oxygen species on oxide materials, which moving on from the Che's pioneering works includes noteworthy results obtained during the years by other researchers. In particular, applications of two powerful techniques such as electron paramagnetic resonance (EPR) and photoluminescence (PL) for detailed characterization of paramagnetic (O^-, O_2^-, O_3^-) and diamagnetic surface oxygen varieties (O^{2-}_{surf}), respectively, are addressed here. Classification and insights into the formation pathways of these species on various oxide surfaces, as well as their involvement in model and real gas/solid and liquid/solid reactions of catalytic and photocatalytic relevance is also considered. Finally, the relationship between the thermodynamic and kinetic Bronsted basicity of low coordinated O^{2-}_{Lc} anions is discussed, on the basis of Che's fundamental studies and on recent developments.

1. Introduction

The chemistry of oxygen species at the surface of metal oxides represents one of the most original Michel Che's contributions to the research in the area of surface chemistry related to catalysis, since the beginning of his activity in the late sixties. The scientific context, at that time, was the development of a rational and systematic approach to catalytic phenomena favoured by the advent of increasingly sophisticated physical techniques for the investigation of solid surfaces. This idea is clearly stated in the abstract of one of the two seminal review papers [1,2] published in the early eighties together with Antony Tench, true milestones in the field of surface oxygen paramagnetic species where it is asserted: "There is a need for a holistic approach to the reaction mechanism which combines both a study of the intermediates by a variety of techniques coupled with an overall analysis of the reaction pathway".

The instrument of choice was, in this case, Electron Paramagnetic Resonance. This technique showed a strong potential in describing the nature and features of defects present in the solid, especially those generated by various types of high energy irradiation. The intuition of few pioneering scientists, Jack Lunsford, Antony Tench and Michel Che, was that this approach could be adopted to study the surface of solids and in particular of oxides.

The early activity of Michel Che started with his PhD thesis in Lyon, 1968, continued in Princeton in the laboratory directed by J. Turkevich and, from 1971 to 1975 in the Institut de Recherches sur la Catalyse (CNRS) in Lyon where he enlivened a collective activity on EPR and surface chemistry involving also Claude Naccache, Younes Ben Taarit and Jacques Védrine. All this work devoted to radical oxygen species also convinced Michel Che and his collaborators that the coordination sphere of oxygen anions, whatever their nature, plays a major role in

* Corresponding author.
E-mail address: helene.pernot@sorbonne-universite.fr (H. Lauron-Pernot).
[1] Sorbonne Université, Laboratoire de Réactivité de Surface UMR 7197, case 178, 4 Place Jussieu, 75252 Paris Cédex 05, France.

https://doi.org/10.1016/j.jcat.2020.10.011
0021-9517/

governing their reactivity. Still in the review published in 1982 with A.J. Tench [1], he underlined some papers already showing that the electron donating power of O^{2-} anions towards oxygen was strongly linked to their coordination defects (O^{2-}_{Lc} for Low Coordinated oxide ions, L < 5) that could be evidenced by photoluminescence (PL) spectroscopy. This method, widely utilized in exploring the molecular photochemistry for a long time, was applied later (in the 70′s) for the characterization of the active sites of the heterogeneous catalysts related to adsorption, catalysis, and photocatalysis [3–5].

Thus, from the very beginning of his studies, Michel Che pioneered the development and the coupling of EPR and PL characterization techniques to reveal, at a molecular scale, the nature of oxygen species that was of first interest for reactivity applications like alkanes or alcohols mild oxidation and more recently in the field of the characterization of the basicity of the materials.

2. Formation and classification of reactive oxygen species on catalytic surfaces

Oxygen plays an essential role in catalysis, not only as a reactant of many important catalytic oxidation reactions, but also as a component of most heterogeneous catalysts and photocatalysts [6–9]. The triplet ground state of the oxygen molecule, $^3\Sigma^-_g$, creates a spin barrier for its reactivity with closed-shell organic and inorganic molecules. It may be, however, circumvented by activation via oxygen coordination (formation of covalently bound metal-oxo units) or by successive reduction via electron transfer steps (formation of distinct ionic moieties). The resultant anionic reactive oxygen species (ROS) on oxide surfaces can be classified into suprafacial (O^-_{ads}, $O^-_{2\,ads}$, $O^{2-}_{2\,ads}$, $O^-_{3\,ads}$), intrafacial (O^-_{surf}, O^{2-}_{surf}) and mixed interfacial ($O_{surf}O_{ads})^{2-}$ categories [1,2,10]. In addition, we may also distinguish clathrated O^-_{cage}, O^-_2, $O^{2-}_{2\,cage}$ and even O^{2-}_{cage} entities, observed in nanoporous materials such as mayenite ($12CaO\text{-}7Al_2O_3$) [11,12].

On the catalytic surfaces, formation of the anionic ROS is usually epitomized via series of consecutive reduction/dissociation steps,

$$O_{2(g)} \rightarrow O^-_{2ads} \rightarrow O^{2-}_{2ads} \rightarrow O^-_{ads} \rightarrow O^{2-}_{surf} \quad (1)$$

where cationic redox centers act as prime electron donors [6,7,13]. Such stepwise reduction changes the electron and proton affinities of the resultant oxygen species, controlling their actual electrophilic, nucleophilic and electroprotic behavior in catalytic reactions. Yet, this basic scheme is not always rigorously followed [14]. The first step only, formation of superoxide species, is adequately documented [2,15–17]. The O^{2-}_2 adspecies may be produced, alternatively, directly via two electron transfer upon adsorption onto dual cationic redox sites present, e.g., on the surface of spinels [18] or through superoxide spillover and dismutation, observed in the case of catalysts with scarce isolated cationic redox centers, exemplified by transition metal ions supported on insulating oxides [17,19,20]. Another quite common pathway includes back electron transfer to the parent cation, and accommodation of the atomic oxygen moiety on the adjacent O^{2-}_{surf} anion (e.g., $Co^{3+}O^- + O^{2-}_{surf} \rightarrow O^{2-}_2 + Co^{2+}$ [21]). It provides the pathway for surface diffusion of atomic ROS, which is crucial for the Langmuir-Hinshelwood-type reactivity [6,8,21] The interfacial O^{2-}_2 intermediates may also be produced via O_2 (or N_2O) interaction with the basic O^{2-}_{surf} surface sites acting as anionic redox centers ($½\ O_2 + O^{2-}_{surf} \rightarrow O^{2-}_2$) [22]. The O^- species, in turn, are often generated upon N_2O adsorption via dissociative electron transfer [17,23,24]

$$N_2O + e^- \rightarrow O^-_{ads} + N_2 \quad (2)$$

or as a hole O^-_O (h^+_{VB}) intrafacial centers, produced via photochemical charge separation ($0 \rightarrow e^-_{CB} + h^+_{VB}$) [25–27].

Valence pining, exemplified by the classic $Li^+_y\ Mg^{2+}_{1-y}\ O^{2-}_{1-y}O^-_y$ (Li_y' $Mg^{\times}_{1-y}O^{\times}_{1-y}O^{\cdot}_y$) catalyst used for methane coupling provides another pathway of generation of the intrafacial O^- centers [28].

Because the O^{2-} adspecies are thermodynamically unstable on the surface, deep 4-electron reduction of dioxygen is only possible by mediacy of anionic vacancies ($½\ O_2 + 2e^- + V^{\cdot\cdot}_O \rightarrow O^{\times}_O\ (O^{2-}_{surf})$, by participation of suprafacial protons ($½\ O_2 + 2e^- + H^+ \rightarrow OH^-_{ads}$) or concomitant formation of cationic vacancies (e.g., $½\ O_2 + 2e^- + M^{\times}_M \rightarrow (O^{2-}M^{2+})_{surf} + V''_M$). The $M^{\times}_M$ cation is extracted from its framework positions onto the surface to stabilize and charge balance the deeply reduced surface O^{2-} species, leaving the bulk V''_M vacancy behind. Such mechanism leads to gradual stoichiometric oxidation of the catalyst with formation of oxides often with gross amount of cationic vacancies, as observed in the case of maghemite [29].

In the solid/liquid environments reactive oxygen species can be generated upon interaction of H_2O_2 with redox oxides via the Fenton-type mechanism [30,31]. A more involved way occurs through H_2O_2 interaction with amorphous oxides of high valent d^0 transition metal ions [32], according to the electroprotic mechanism ($\equiv Zr + -HO^-_2 + H_2O_{2(aq)} \rightarrow {\cdot}OH_{(aq)} + \equiv Zr^+\text{–}O^-_{2\ (ads)} + H_2O$). Another important route of ROS formation is related with the photocatalytic reduction where electrons promoted to the conduction band (e^-_{CB}) are scavenged by adsorbed O_2 or N_2O to produce the corresponding O^-_2, O^- or O^-_3 radical anions [25,33]. Paramagnetic oxygen species may also be produced via oxidative pathway upon photogeneration of holes in the valence band ($O^{2-}_{surf} + h^{\cdot+}_{VB} \rightarrow O^-_{surf}$). All those species may coexist on the surface, and interact mutually or with protons available on the catalytic surfaces to produce various reactive oxygen species (ROS), which participate in concert or successively in the catalytic oxidation processes, depending on the actual reaction conditions [6,7,34].

Alternative to electron transfer route of oxygen activation is constituted by oxygen atom transfer with formation of covalently bound mono- and multi-metal-oxo species of two generic kinds $M(d^0)$=O, and $M(d^n)$=O. In the latter case strong spin polarization of the M=O bond by the adjacent d^n electrons gives rise to appearance of very reactive cores, capable to activate the C–H bonds of methane even at room temperatures. A spectacular example is provided by the ferric FeO^{n+} unit, known as alfa-oxygen [35]. The $M(d^0)$ = O units may, in turn, be raised into highly active triplet $[M(d^1)\text{–}O^-]$ state via UV-irradiation [13,36]. Finally, owing to their relevance for gas and liquid phase oxidation reactions, we may add into the reactive oxygen species also the protonated forms of O^-_2 ($\cdot HO_2$) and O^- ($\cdot OH$), as well as peroxy radicals produced via spin pairing between the $\cdot R\uparrow$ and $\uparrow\uparrow O_2$ moieties ($ROO\cdot$), which play an important role in the photocatalytical reactions [25,37]. However, in the following chapters, for the sake of brevity, we focus our attention on the ionic oxygen species either paramagnetic or not.

We thus review first the work made on EPR and PL spectroscopies that were developed to characterize these species then we describe the main results obtained on their behavior from oxidation reactions intermediates to basic sites. The systematic analysis of the literature before 1983 is contained in the mentioned two review papers [1,2] while for the activity since then, we will consider selected examples from both Che's group and other groups related to him without the presumption of a systematic analysis of all published papers. It will be

easy to recognize in the proposed examples the importance of Michel Che's endless activity and the sign of his scientific legacy to the next generations of researchers.

3. Paramagnetic oxygen species - EPR characterization

For the purposes of the present article it is worth mentioning, that the main innovations in the field of EPR after the eighties are related to an improved quality of the classic continuous wave (CW) instrumentation, to the availability of sophisticated computer programs for simulation of EPR spectra and to the advent of pulse-EPR techniques that have introduced a significant extension of the region probed around the paramagnetic center. Last but not least, a special role has been played by the jump in the accuracy of theoretical calculations of magnetic parameters due to the advent of DFT methods that have become a tool of increasing importance to support experimental research [38].

3.1. Mononuclear oxygen species

The most common species of this type is the O^- ion which can be seen either as the deprotonated form of the hydroxyl $OH^\bullet$ radical or as an oxide O^{2-} ion trapping a hole. The electron configuration of the O^- radical is $[2p_x^2, 2p_y^2, 2p_z^1]$ and the corresponding elements of the ***g*** tensor [39], neglecting second-order terms, are

$$g_{zz} \approx g_e \quad g_{xx} = g_e + 2\lambda/\Delta E_1 \quad g_{yy} = g_e + 2\lambda/\Delta E_2 \tag{3}$$

where λ is the spin-orbit coupling constant for atomic oxygen and ΔE the difference between the ground and the first excited state *i.e.* the energy cost to promote the hole from $2p_z$ to another p orbital (see crystal field splitting diagrams in Scheme 1). In the common case of an axial symmetry of the crystal field the $2p_x$ and $2p_y$ orbitals are degenerate and the tensor becomes

$$g_{zz} = g_{||} \approx g_e \quad g_{xx} = g_{yy} = g_\perp = g_e + 2\lambda/\Delta E \tag{4}$$

with $\Delta E_1 = \Delta E_2 = \Delta E$.

The surface O^- species on metal oxides has been observed both upon reductive decomposition of N_2O and as a result of photoexcitation with consequent charge separation. Surprisingly, there is no clear evidence about the formation of this species during the reduction/dissociation process in Eq. (1). The decomposition of nitrous oxide has been followed at the surface of electron-rich MgO, a highly ionic insulating oxide widely used as model solid. All ions in the bulk are 6-coordinated while, surface cations and anions have coordination numbers from 5 to 3 being exposed in various topological locations. Electron-rich surfaces of alkali earth oxides contain unpaired electrons trapped by low coordination ions (at terraces -**T**, steps - **S**, edges - **E**, corners - **C**) or by particular morphological locations such as the reverse corners (**RC**) [40]. The heterogeneity of the surface traps, barely appreciable in their EPR spectra, is revealed by the O^- probe resulting from the reaction with nitrous oxide (Eq. (2)) that gives rise to complex spectra. These are amenable to the overlap of several axial signals corresponding to a variety of O^- suprafacial species [41,42]. Successive work has rationalized these observations by theoretical calculations of the reaction (2) on the crystal surface containing trapped electrons [43]. The results indicate that the O^- species have an electron spin density highly localized in a p orbital and ΔE values ranging from few tenths of eV to about 1 eV. The ΔE values progressively increase for O^- ions moving from **T** to **E**, **C** and **RC** sites.

The interfacial O^- centre has been widely investigated as it results from photoexcitation of a metal oxide. This process is crucial in photocatalytic phenomena since the interfacial O^- centre, a surface oxide ion bearing an electron hole, is extremely reactive and entails the oxidative channel in photocatalytic reactions. The study of photoexcitation is not limited to semiconducting oxides employed in photocatalysis. In the case of model oxides such as MgO irradiation studies followed by EPR gave the opportunity of describing energy transfer phenomena at the surface as reported by Knoezinger and co-workers [44,45] who showed that excitation with monochromatic light of oxide anions located either on edges (225 nm) or on corners (269 nm) ends up in the formation of a unique tri-coordinated O^- species (O^-_{3c}) at corners of the cubic crystals. Similar evidence was obtained by X-ray irradiation under vacuum of polycrystalline MgO. In this case an EPR spectrum composed by two sharp signals with narrow spectral lines [43] was observed (Fig. 1).

The first one (close to g_e) is due to trapped electrons while the second one is due to the above mentioned O^-_{3c} hole center trapped at the corner sites with $g_\perp = 2.0357$. These particular sites, are the ultimate sink of the photogenerated holes on MgO. Because of the very low line-

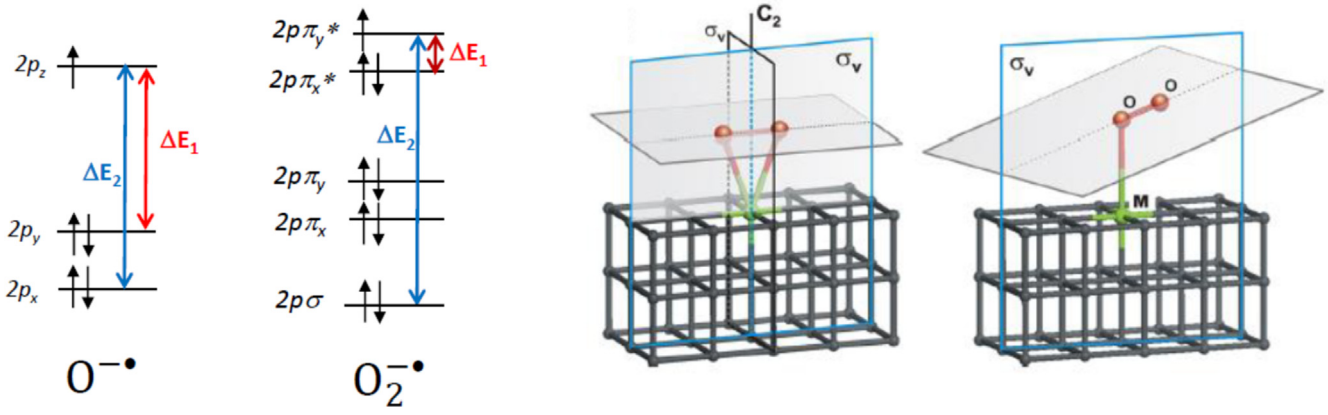

Scheme 1. Energy levels of O^- and of O_2^- radical ions and schematic view of η^2 side-on (left) and of η^1 end-on (right) superoxide adducts.

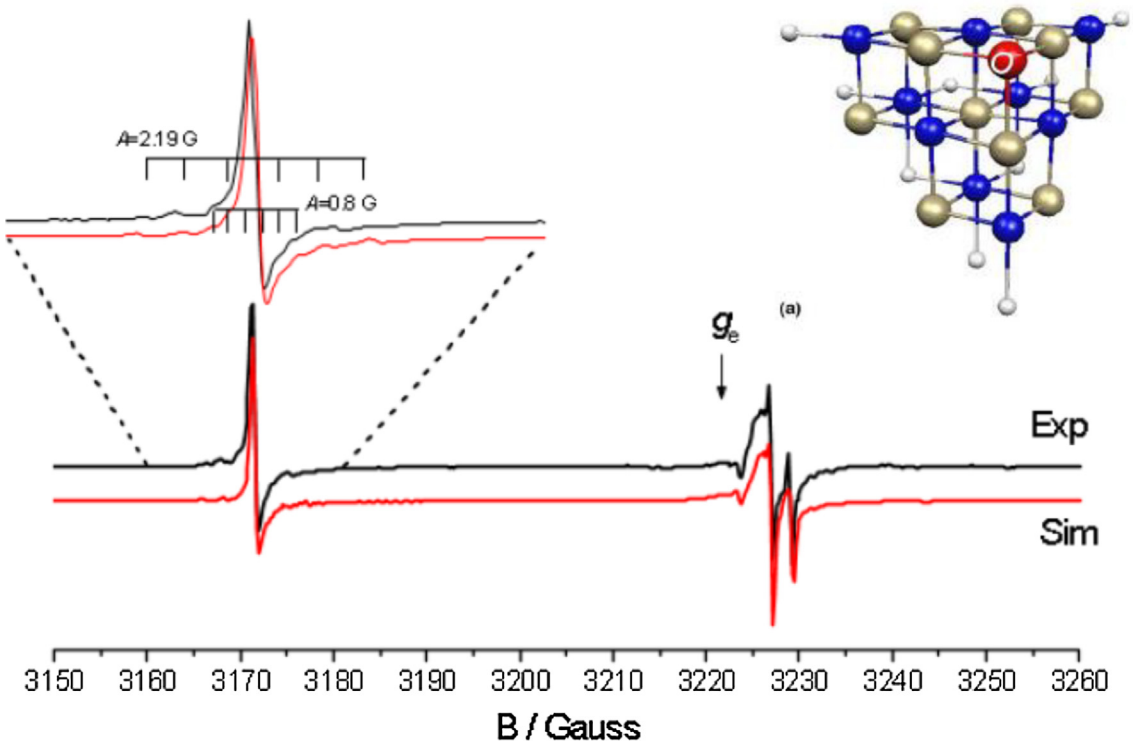

Fig. 1. EPR spectrum of trapped electron (right) and trapped hole O^- centres (left) formed at the surface upon X-ray irradiation of MgO under vacuum. Inset: magnification of the superhyperfine structure of O^- due to ^{25}Mg. Top right: sketch of the corner site hosting the hole. (Figure adapted from Ref. [43]).

width of the O^-_{3c} signal it was possible to observe a superhyperfine structure on the perpendicular component due to ^{25}Mg (nuclear spin I = 5/2, 10% natural abundance) in the first coordination sphere (Fig. 1, stick diagram). The same experiment was performed on a ^{17}O enriched MgO sample. The resulting spectrum has allowed the first determination of the hyperfine tensor for the three coordinated $^{17}O^-_{3c}$ center [46]. The hyperfine constants are $A_\perp$= 1.9 mT and $A_\parallel$ = 10.56 mT, quite close to those reported for $^{17}O^-$ obtained from $N_2{}^{17}O$ decomposition on electron-rich MgO [47,48].

Investigations on the behaviour of photoexcited charge carriers in TiO_2 have particular importance for the paramount role of this oxide in photocatalysis. The formation of trapped electron and trapped hole centers have been investigated in aqueous suspensions of colloidal TiO_2 [49,50] as well as on materials kept under vacuum [27]. In both cases the photo-formed charge carriers are stabilized at the surface under the form of O^- and Ti^{3+} ions respectively. The stabilization of holes at the surface of titania is favoured by the presence of water at the interface. In an investigation carried out coupling EPR and ENDOR (Electron Nuclear Double Resonance) it has in fact been possible to distinguish the features of O^- centers in subsurface sites of TiO_2 from those of surface O^- [51] determining the distance between the hole centers and the protons of coordinating water molecules.

A special type of O^- species are those that are undetectable because of a highly symmetric environment (small or nearly null ΔE value in Eqs. (3) and (4)) or because of their mobility. In the case of Na doped CaO their presence has been indirectly monitored by EPR. In calcium oxide, the presence of aliovalent Na^+ ions is compensated by an equivalent number of hole O^- centres that are not EPR-active. However, by adsorption of molecular oxygen at low temperature, an intense signal due to ozonide O_3^- ions shows up [52]. The ozonide radical ion is formed according to the $O^- + O_2 \rightarrow O_3^-$ reaction that requires the presence of O^- at the surface. Remarkably, by a careful control of the surface ozonide decomposition (vacuum annealing at 323 K) the O^- species become revealed ($g_\perp$ = 2.0175) in a restricted time interval then progressively disappears upon prolonged annealing.

3.2. Molecular oxygen species: the superoxide ion

Among the molecular surface oxygen species, apart from some papers concerning the ozonide O_3^- ion [53] the O_2^- superoxide ion is by far the most investigated one being the first step of the reduction of molecular oxygen. EPR techniques have provided along the years a great deal of information on the structural features and on the behaviour of this species because of the diagnostic value of the magnetic ***g*** and ***A*** tensors [16]. The superoxide moiety can be linked at the surface of an oxide by different types of chemical interactions that will be examined in the following.

3.2.1. Ionic bonding in adsorbed superoxide - EPR features and magnetic tensors

The ionic bonding with surface cations is the more common form of interaction between superoxide and metal oxides. The O_2^- radical ion has the electronic structure typical of 13-e^- diatomic radicals [17] sketched in Scheme 1. The ***g***-tensor of these species was first derived in the case of the O_2^- defect confined in the bulk of alkali halides [54]. A simpler form of ***g***-tensor obtained neglecting second order interactions, relates the principal values of the tensor to the energy splitting between orbitals:

$$g_{xx} = g_e \quad g_{yy} = g_e + \frac{2\lambda}{\Delta E_2}; \quad g_{zz} = g_e + 2\lambda/\Delta E_1 \tag{5}$$

with $g_{zz} > g_{yy} > g_{xx}$. The most common form of adsorbed superoxide in ionic interaction with the surface shows a η^2 (side-on) structure with C_{2v} symmetry (Scheme 1). The z direction corresponds to the internuclear molecular axis and the *y* direction is perpendicular to the surface. ΔE_1 is the splitting between the two $2p\pi^*$ antibonding orbitals, degenerate in the O_2 molecule, caused by the crystal field splitting exerted by the adsorption site. The unpaired electron is localized in one of the two $2p\pi^*$ orbitals. The relatively low value of ΔE_1 gives rise to a marked sensitivity of the g_{zz} value to the surface field of the adsorbing cation that depends on its charge to radius ratio. This factor makes adsorbed O_2^- an excellent probe of the oxide surfaces. It is in fact possible, for instance, to observe distinct g_{zz} components when superoxide is adsorbed on different cationic sites at the surface of complex oxides. For example, investigations of TiO_2/ZrO_2 mixed systems of various compositions have clearly evidenced the formation of two fractions of surface adsorbed O_2^- ions on Zr^{4+} (g_{zz} = 2.030) and Ti^{4+} (g_{zz} = 2.022) respectively [55]. The sensitivity of the method is however even higher since it is possible, in some cases, to distinguish adsorption sites of the same nature but located in distinct topological region of the investigated crystal. In each location, because of the different coordinative environment, the adsorbing positive ions assume a different Madelung potential. A systematic EPR study of surface superoxide speciation on MgO (using different chemical and physical routes to generate the radical ion) has allowed the assignment of three main species having g_{zz} values of 2.0640, 2.0770 and 2.0910. These correspond to O_2^- ions adsorbed on 3-coordinated cations (Mg^{2+}_{3c}) at corner sites, on Mg^{2+}_{4c} at edges and on Mg^{2+}_{5c} on terraces respectively [56,57].

A particularly significant example of the use of superoxide as a surface probe of ionic systems has been reported in the case of magnesium oxide containing surface adsorbed cesium atoms [58]. Contacting the Cs-MgO system with molecular oxygen, superoxide ions are formed by electron transfer from the adsorbed Cs atom. A fraction of the resulting O_2^- remains on top of Cs^+ ions while a second fraction undergo spillover to the surface where it is stabilized by two distinct types of Mg^{2+} ions. The EPR spectrum in Fig. 2 precisely describes the system after reaction, showing an highly resolved g_{zz} region with components at g_{zz} = 2.091 (Mg^{2+}_{5c}), g_{zz} = 2.077 (Mg^{2+}_{4c}) and g_{zz} = 2.1197 (Cs^+) [59]. Remarkably each component of the O_2^-–Cs^+ species is split in 8 lines (stick diagram in Fig. 2) due to the superhyperfine interaction with the ^{133}Cs nucleus (nuclear spin I = 7/2, 100% natural abundance). Other examples of superhyperfine interaction related to O_2^- adsorbed on MgO were reported in the case of O_2^-–H^+ [60]) and in that of O_2^-–Na^+ [61].

Isotopic enrichment of molecular oxygen with ^{17}O (I = 5/2) is commonly used in the investigation of surface superoxide in order to observe a hyperfine interaction. The analysis of the ^{17}O hyperfine structure allows discernment between O_2^- species with magnetically equivalent and non-equivalent nuclei [2,16]. Since a structural equivalence must correspond to the magnetic equivalence, in the former case the two oxygen atoms are symmetrically (η^2 side-on structure) adsorbed on top of the surface cation. The first example was reported by Tench in 1968 in the case of O_2^- formed via O_2 absorption on an electron-rich MgO surface [62]. The reported spectrum clearly shows a sextet of lines centred on the g_{xx} component due to the $^{17}O^{16}O^- = {}^{16}O^{17}O^-$ equivalent isotopomers overlapped with a set of 11 lines due to the $^{17}O^{17}O^-$ one, thus enabling the authors to assert the magnetic equivalence of the two nuclei. However, the resolution of the spectrum was sufficient to measure the A_{xx} component only, while A_{yy} and A_{zz} remained undetermined. The first comprehensive analysis of a surface $^{17}O_2^-$ spectrum was achieved more than 30 years later with an experiment performed on highly crystalline materials [63]. It was possible, in this way, to measure the complete hyperfine tensor and to determine an electron spin density on the $2p\pi^*$ orbital of 0.99 indicating the total electron transfer from the surface electron traps to the adsorbed oxygen.

The non-equivalence of the two oxygen atoms in adsorbed superoxide was firstly proposed in the case of O_2^- – Mo^{6+} [64] on the basis of a hyperfine structure exhibiting two sextets of lines with different coupling constant. In principle the observed pattern could also be due to the simultaneous presence of two distinct adsorption sites with different degree of metal-to-oxygen electron transfer. Recent analysis [65] have however demonstrated that there is a unique site where the superoxide adsorbs with a low-symmetry structure and an inequivalent

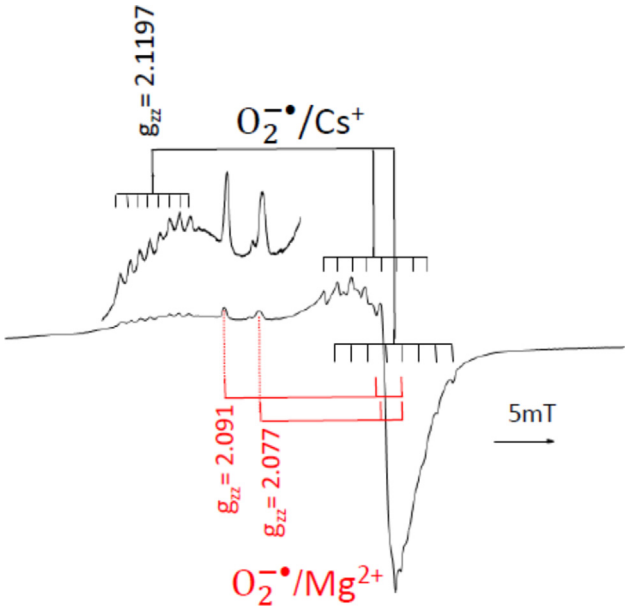

Fig. 2. EPR spectrum of superoxide ions formed upon O_2 adsorption on Cs-MgO. The stick diagram evidence the superhyperfine structure due to ^{133}Cs. Figure adapted from Ref. [59].

electron spin density distribution over the adduct. The reason of such non-equivalency is not yet clear. Either the role of particular surface morphological features or that of covalent interactions with the transition metal ion (TMI) centre, have been invoked in this case.

3.2.2. Covalently bound adsorbed superoxide - reversibility of the interaction

The covalent interaction between oxygen and TMI at the surface is an alternative to the purely ionic bonding as shown in some examples appeared in the literature starting from the late eighties. The first case concerns the cobalt-dioxygen chemistry occurring at the surface of CoO-MgO solid solutions that shows clear analogies with similar phenomena in molecular systems. The contact of oxygen with the activated solid at about 100 K leads to the formation of a EPR spectrum that is the overlap of two distinct signals both characterized by an hyperfine interaction with ^{59}Co nuclei (I = 7/2) [66]. Rising the temperature to 290 K the spectrum reduces its complexity since a fraction of the adsorbed oxygen undergoes spillover forming a classic O_2^-/Mg^{2+} species, while a second fraction generates a novel paramagnetic Co–O_2 adduct slightly different from those present at low temperature. The three Co-O_2 complexes were identified as bent η^1 end-on adducts similar to those formed by square pyramidal low spin Co^{2+} complexes. The analogy between the surface Co-O_2 adduct and molecular complexes was also found in the behaviour upon oxygen pressure. The oxygen adsorption on the CoO-MgO systems is in fact fully reversible and pressure dependent like in the case of the mentioned molecular oxygen carriers characterized by a weak metal - oxygen bond. The CoO-MgO system can thus be considered as the first example of a heterogeneous oxygen carrier. The chemical bond in these particular adducts was investigated also by adsorption of ^{17}O enriched molecular oxygen to prove the non-equivalent nature of the two oxygen atoms and the η^1 end-on structure (C_s symmetry) of the adduct. The chemical bonding was described in terms of a substantial cobalt-to-oxygen electron transfer forming an adduct schematically described as Co^{3+}–O_2^-. The ^{59}Co hyperfine structure derives from the main contribution of a direct electron donation between the $2p\pi_x^*$ antibonding orbital of the oxygen molecule to the d_{xz} cobalt orbital that form the molecular orbital hosting the unpaired electron [67].

A new type of superoxide covalent adduct was found, more recently, investigating the interaction of molecular oxygen with ZSM-5 zeolites containing Ni^+ ions [68]. Monovalent nickel ions are paramagnetic ($3d^9$ configuration) and exhibit a typical EPR spectrum that vanishes by contact with O_2, in parallel with the appearance of a new signal of adsorbed superoxide (Fig. 3a). This signal, however, differs from those typical of the classic ionic interaction (Section 3.2.1, Eq. (5)) because of the relatively high values of the three principal components of the $\boldsymbol{g}$ tensor (g_{xx} = 2.0635, g_{yy} = 2.0884, g_{zz} = 2.1675). The spectra obtained using ^{17}O enriched O_2 indicate that the two oxygen atoms are magnetically equivalent thus pointing to a η^2-side on structure (Fig. 3b). The hyperfine coupling however occurs along the direction of the intermediate g component (g_{yy}) instead of along g_{xx}, as it occurs in ionic adducts. Both anomalies are due to a relevant role of covalent interactions between the side-on oxygen moiety and the 3d orbitals of the nickel ion that leads to a substantial quite homogeneous redistribution the electron spin density in the triangular array of the η^2-NiO_2 system. The singly occupied molecular orbital (SOMO) is based on a δ-type overlap between the antibonding $2p\pi^*$ oxygen molecular orbital and the $3d_{x2-y2}$ orbital of the nickel ion (Fig. 3c). The interaction is not reversible and the paramagnetic complex decomposes upon evacuation at 373 K without reappearance of the Ni^+ signal.

Very recently, unprecedented examples of η^2side-on reversible oxygen adducts have been reported in the case of indium oxide [69] and of three mixed oxide materials containing cerium ions. In the case of Ce-$ZrTiO_4$ and Ce-ZrO_2, cerium ions are diluted in the oxide matrix forming solid solutions [70,71], the CeO_2/TiO_2 system is instead biphasic with heterojunctions between the two oxides [72]. The solids,

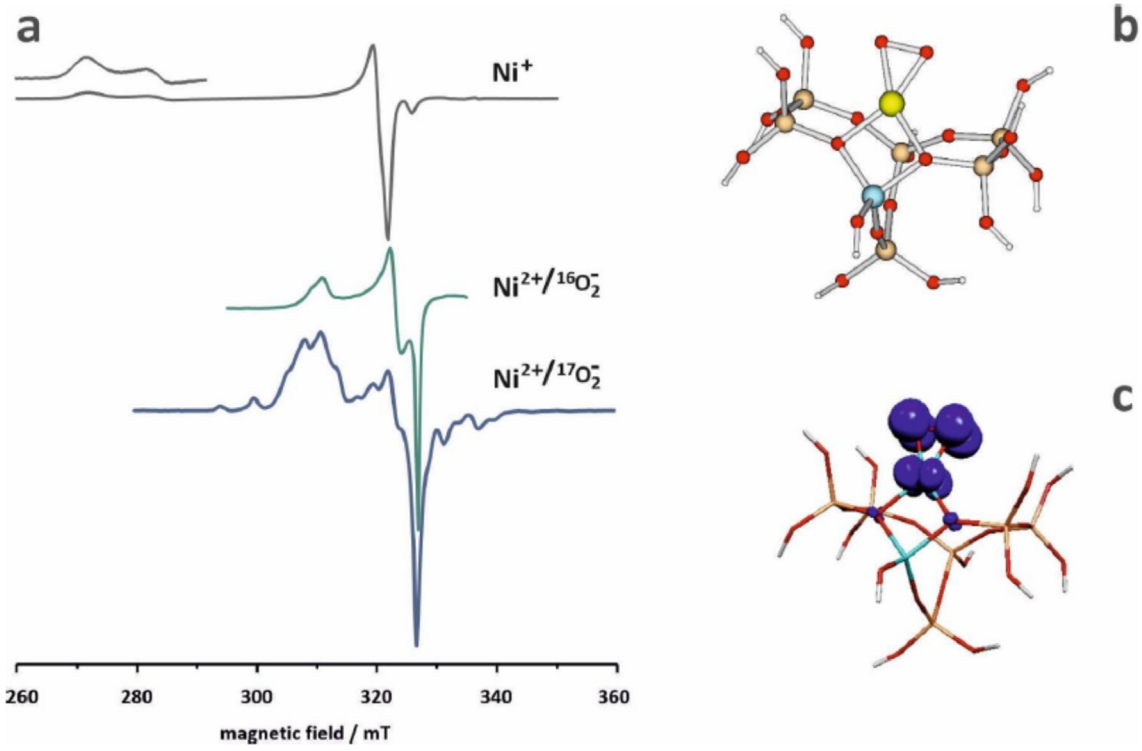

Fig. 3. EPR spectra (a) of Ni^+ ions in ZSM5 zeolite and of the oxygen adduct obtained using $^{16}O_2$ and $^{17}O_2$ respectively. Structure (b) and MO scheme of the Ni–O_2 adduct (c). Figure adapted from Ref. [68].

after an oxidative calcination treatment at high temperature, adsorb molecular oxygen giving rise to EPR signals very similar in the three cases and due to superoxide species. Ce^{3+} ions (paramagnetic but not detected by EPR) have been observed by XPS (in the case of CeO_2/TiO_2) suggesting a partially reduced state of the solid in which the presence of Ce^{3+} ions is compensated by oxygen vacancies. Ce^{3+} centres are responsible of the electron transfer towards oxygen to form a O_2^-/Ce^{4+} adducts whose EPR signal has an atypical line shape due to the fact that the three principal values of the ***g***-tensor are very close one to another (Fig. 4). The ***g*** tensor elements in the three cases are g_{zz} = 2.026, g_{yy} = 2.022, g_{xx} = 2.013. Remarkably, the observed ***g***-tensor differs from that observed for superoxide on bare CeO_2 and does not correspond to the ionic model of surface O_2^- (Eq. (5)), suggesting, once again, a role of covalence in the chemical bond. However, at variance with the case of pristine CeO_2 and of η^2-NiO_2, the adsorption of oxygen as superoxide is fully reversible and pressure dependent indicating a weak interaction between the molecule and the adsorption centre. These experimental findings were fully confirmed by DFT results on the Ce-ZrO_2 system [71] that point out the formation of a symmetric side-on adduct with a binding energy of 0.45 eV, a negligible activation energy and a nearly complete electron transfer on oxygen (Fig. 4). The three cases illustrated herein are therefore further examples of heterogeneous oxygen carriers unravelled by EPR showing however symmetric coordination of the oxygen molecules.

3.2.3. Superoxide ions and other molecular species at surfaces and in cavities

After the initial rapid growth of studies on surface paramagnetic oxygen species that led to their methodical classification available in Refs. [1] and [2], the activity in the field became less systematic and focused on specific research topics. It is worth of briefly mentioning, for instance, the case of titanium dioxide. This oxide, highly important for its photochemical properties has been studied for its ability to form surface superoxide by photoexcitation in its pristine form [26,27] as well as when sensitized with particular dyes [73]. Different kinds of studies were instead devoted to investigate the defective features of the surface. In this way it has been possible to describe the existence of two distinct types of surface ionic superoxide on TiO_2 assigned to side-on adducts stabilized on oxygen vacancy, [V_O – O_2^-] and on non-vacancy sites (Ti^{4+} – O_2^-) respectively [74,75].

Zirconium dioxide is a ceramic material widely employed in materials science and in catalysis. The formation of superoxide species on ZrO_2 (g_{zz} = 2.0336, g_{yy} = 2.0096 and g_{xx} = 2.0034), that is favoured by a partial hydration of the surface [76] has been also investigated after modifications of either the bulk with yttrium [77] or of the surface with sulphate ions forming sulphated zirconia, a heterogeneous catalyst active in acid-catalysed reactions [78]. In order to control the state of surface defects, the formation of superoxide has been monitored on both CeO_2 [79] and in ceria based materials [80,81]. The EPR spectral features were related to different types of surface vacancies such as single or associated vacancies.

Oxygen paramagnetic species located within the bulk of nanoporous oxides recently have attracted the attention of researchers. A system of reference in this field is Mayenite ($12CaO{\cdot}7Al_2O_3$). Interestingly, the cage mobile ions can be replaced by other negative entities including paramagnetic O_2^- and O^- radical ions capable of giving to the solid additional properties as an oxidation catalyst. EPR has played a crucial role in the characterisation of O_2^- radical ions within the cages in a wide concentration range [82] and the HYSCORE technique was employed to show that O_2^- ions are encapsulated in the proton free cavities of mayenite where they preferentially interact with Ca^{2+} ions [12].

4. Reactivity of surface anion-radical oxygen species

Interaction of dioxygen and oxygen donor molecules such as N_2O or NO_2 used as oxidants in catalysis give rise to formation of various surface reactive oxygen species that may participate in a variety of ways in catalytic reactions. Among them we may distinguish two main categories: (i) catalytic processes where ROS are incorporated in the reaction products (selective and total oxidation) [6–8], and (ii) reactions where dioxygen evolution step plays a key role (N_2O, NO and O_3 decomposition, $^{16}O_2/^{18}O_2$ isotopic exchange) [83]. Generally,

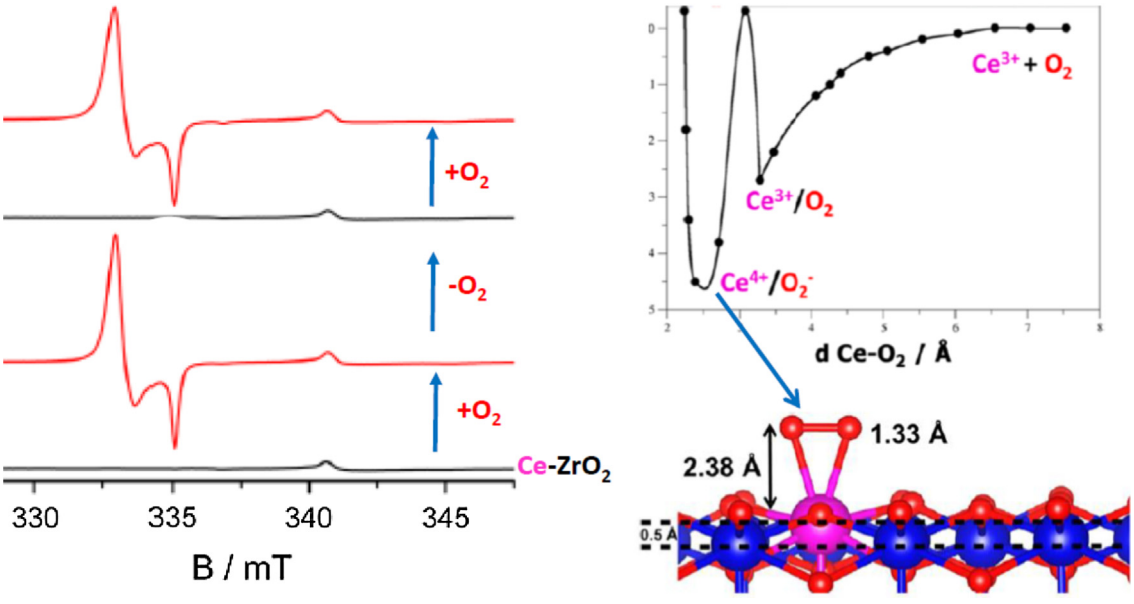

Fig. 4. EPR spectra (left) showing the adsorption of O_2 on Ce-ZrO_2 with reversible formation of a superoxide adduct. Right: calculated potential energy profile as a function of the Ce – O_2 distance and calculated scheme of the η^2 side on reversible adduct. Figure . adapted from [71]

hydrocarbon oxidation processes have been classified into the nonselective electrophilic oxidation, involving radical oxygen intermediates (O_2^-, O^-) that lead to total oxidation, and the selective nucleophilic oxidation, where the O^{2-} anions play the key role [6]. It should be noted, however, that such dichotomic division is not rigorous in the light of the latest results. Several examples are provided, which document well selective oxidation reactions involving the O_2^- or O^- intermediates that are operating at low temperatures in catalytic gas-solid [84] and catalytic/photocatalytic solid-liquid systems in particular [85] EPR technique has often been applied to monitor surface reactions of oxygen species, but its applicability is limited to studies of radicals in the low temperature processes. Since most of ROS are unstable in nature, it is usually difficult to monitor directly their behavior at higher temperatures where they appear as transient intermediates [65].

Generally, the reactions involving anion-radical oxygen species can be classified in (i) exchange and charge disproportionation processes, (ii) ROS addition reactions, and (iii) reactions initiated by hydrogen atom/proton abstraction or (iv) by hole transfer processes.

4.1. Exchange and charge disproportionation reactions

Isotopic exchange and ROS disproportionation reactions are among the simplest processes that are probing ROS surface dynamics and their latent reactivity in catalytic research. Involvement of O_2^- in isotopic exchange has been revealed clearly by EPR technique upon contacting the $^{16}O_2^-$ radical trapped on the surface of a supported MoO_x/SiO_2 catalyst with the gas phase $^{17}O_2$ [65]. Development of the characteristic hyperfine pattern due to the singly and doubly labelled dioxygen isotopomers, implies the following reactions $^{16}O_{2\ (ads)}^- + {}^{17}O_{2(g)} \rightarrow {}^{16}O_{2(g)} + {}^{17}O_{2\ (ads)}^-$ and $^{16}O_{2\ (ads)}^- + {}^{17}O^{16}O_{(g)} \rightarrow {}^{16}O_{2(g)} + {}^{17}O^{16}O^-_{\ (surf)}$ to occur quite readily. Further example is provided by $O_{2\ (ads)}^- + O_{2\ (ads)}^- \rightarrow O_{2(g)} + O_{2\ (ads)}^{2-}$ charge disproportionation. The corresponding second order kinetics of the decay of O_2 species has been observed over the catalysts containing isolated and clustered molybdenum species supported on silica [20]. The reaction takes place via spillover onto the silica support in the case of isolated Mo centers, whereas for larger MoO_x clusters the recombination is confined to the molybdenum moieties, as has been well documented by persistence of the ^{95}Mo hyperfine structure of the decaying superoxide species.

4.2. ROS addition pathways - reactions with small molecules

Monoatomic O^- species regardless of their nature and supra- or intrafacial localization exhibit high chemical reactivity toward small molecules, even at cryogenic temperatures [1,13,17,86]. Suprafacial $O^-_{\ (ads)}$ radicals react readily with small molecules such as O_2, CO, N_2O, in an associative way, producing the corresponding amassed radical intermediates O_3^- (or $O^-{\cdot}O_2$ adducts), CO_2^-, $N_2O_2^-$ [17]. For a model association reactions with dioxygen, an illustrative example is provided by detailed kinetic ($d[O^-{\cdot}O_2]/dt = -k_{-1}[O^-{\cdot}O_2]$) and thermodynamic ($k_1[O^-]n(O_2) \leftrightarrow k_{-1}[O^-{\cdot}O_2]$ equilibrium) study of O reaction with O_2 over the MgO surface [87,88]. In the temperature range of 263–283 K, this reaction leads to the formation of a corresponding $[O^-{\cdot}O_2]$ ozonide radical adduct with ($g_1 = 2.017$, $g_2 = 2.010$ and $g_3 = 2.002$), and the activation barrier of ~ 19 kJ/mol only. Reaction of O^- with O_2 leading to O_3^- ($g_1 = 2.009$; $g_2 = 2.005$; $g_3 = 2.002$) was also observed on the surface of CeO_2/TiO_2 photocatalysts [89], and on MgO surface [53].

Analogous reaction between O and CO performed at 77 K leads to development of CO_2 adspecies with g_1, = 2.0029, g_2, = 2.0016, g_3, = 1.9974, and ^{13}C hfs A_1, = 19.9, A_2, = 24.0, A_3, = 20.7 mT [90]. Similar CO_2^- radicals ($g_1 = 2.0044$, $g_2 = 2.0022$, $g_3 = 1.998$) are produced over the UV-irradiated silica gel upon interaction of CO the with hole O centers at 90–250 K, and the reaction follows the Langmuir-Hinshelwood-type mechanism with an activation energy of 18 kJ/mol [91].

At low temperatures the reactivity of superoxide radicals is usually limited to formation of adducts with most inorganic and larger organic molecules. Several adducts of such type have been identified on the TiO_2 surface by Murphy et al. [65], including $[O_2^-{\cdot}CH_3CN]$, $[O_2^-{\cdot}CH_3OH]$, $[O_2^-{\cdot}C_6H_5CH_3]$ or $[O_2^-{\cdot}CH_3COCH_3]$ entities. These intermediates decompose at temperatures $T > 220$ K.

Superoxide radicals produced upon O_2 adsorption on a $Pt/CeO_2/Al_2O_3$ catalyst may oxidize CO to CO_2 at room temperature ($r_{ox} = k[O_2^-][CO]$), with the rate constant of $k = 2.5 \times 10^{-21}$cm^{3}molecule^{-1}s^{-1} [92]. In the case of Au/ZnO catalyst, reaction between O_2 and CO at ambient conditions leads to the formation of CO_3 radicals with $g_{xx} = 2.002$, $g_{yy} = 2.007$ and $g_{zz} = 2.028$, which upon increasing of the temperature is transferred into CO_2 [93].

4.3. H-abstraction pathways – Reactions with organic molecules

Fundamental investigations into reactivity of surface oxygen species with hydrocarbon molecules using model systems provide a requisite fundamental background for understanding the molecular mechanism of total and selective catalytic oxidation reactions. The O^-, O_2 (or peroxide HO_2, $^{\cdot}RO_2$) radicals may react with the C–H bond containing molecules present in an adsorbed (Langmuir-Hinshelwood mechanism, LH) or in a gas phase (Eley–Rideal mechanism, ER) state. The hydrogen atom or proton abstraction processes resulting from homo- or heterolytic breaking of the C–H bond and formation of the O–H bond is the characteristic feature of such reactions.

All suprafacial and intrafacial O^- radicals observed by EPR have been found as very reactive toward organic molecules [1,13,17,28,94]. The most demanding abstraction of hydrogen atom from CH_4 by suprafacial O radicals (produced from N_2O on MgO surface) [95] and intrafacial hole O^- centers (present in the Li-MgO catalyst) [96] has been observed to occur quite readily, following the ER mechanism ($CH_{4(g)} + O^- \rightarrow {}^{\cdot}CH_{3(g)} + OH^-$). The resultant methyl radicals can escape into the gas phase (at high temperatures), where they couple into ethane molecules, constituting an example of mixed hetero-homogeneous catalysis [97], or can be trapped on the surface in the form of methoxy intermediates ($^{\cdot}CH_3 + O^{2-} + O_2 \rightarrow CH_3O^- + O_2^-$), opening a rather complex network of various reactions, owing to cooperative action of several ROS species [95].

Such collective operation of the O^{2-} and O_2^- oxygen species is well illustrated by oxidation of alkene molecules on the surface of the alkaline earth oxides, where the Lewis basicity of the O^{2-} anions plays the crucial role. The reaction is initiated by surface O^{2-} ions that are apt to break the C–H bond heterolytically via proton abstraction, forming the corresponding carboanion trapped on the surface and the OH^- anion ($R{-}H + O^{2-}_{surf} \rightarrow R^-_{\ (ads)} + OH^-_{surf}$). The former reacts next with the molecular dioxygen via surface intermolecular electron transfer (SIET), giving rise to formation of superoxide and hydrocarbon radicals, detected by EPR technique ($R^-_{\ (ads)} + O_{2(g)} \rightarrow {}^{\cdot}R + O_{2\ (ads)}^-$) [98]. Subsequent reactions such as, $^{\cdot}R + O_{2\ (ads)}^- + H^+_{(ads)} \rightarrow$ ROOH or $^{\cdot}R{-}H + O_{2(g)} \rightarrow {}^{\cdot}ROO$, lead to facile formation of oxygenates, which are easily combustible in the excess of oxygen at higher temperatures. In the particular case of C_3H_6 oxidation over MgO in mild conditions, those reactions lead to formation of acetates, formates and carbonates, and the kinetics is zero order with respect to propene and second order with

respect to superoxide intermediates. This implies operation of the LH mechanism with dual sites for adsorption of both species being involved [99].

Oxidation of methanol over MoO_x/SiO_2 catalyst gives yet another example where O^-, O_2^- and O^{2-} oxygen species are acting in a concerted way to produce formaldehyde as a final product [100]. The reaction is initiated at 210 K by H-atom abstraction from the C–H (sp^3) bond of the coordinated CH_3OH molecule by the O^- co-ligand

$$(CH_3OH + O^-)–Mo^{6+}–O^{2-} \rightarrow [\cdot CH_2OH + HO^-)–Mo^{6+}–O^{2-}] \rightarrow CH_2O + Mo^{5+}–OH^- \quad (6)$$

The transient radical hydroxymethyl intermediate (g_{av} = 2.0034, $|^H A_x|$ = 2.1, $|^H A_y|$ = 2.65, $|^H A_z|$ = 1.05 mT) is immediately converted into CH_2O (detected by QMS) along an electroprotic step engaging ligand to metal electron transfer (LMET) coupled with transfer of the slightly acidic OH proton to the adjacent surface O^{2-} site. The corresponding kinetic curves of O^- disappearance concerted with Mo^{5+} formation are shown in Fig. 5a, whereas the concomitant spin density transfer from the ligated O^- radical to the sp^2-C atom of the nascent $\cdot CH_2OH$ intermediate during the H-abstraction process is illustrated in Fig. 5b. The reaction occurs according to the first-order kinetics with k_{obs} = 0.038-min^{-1}. In the presence of dioxygen, a SIET reaction ($\cdot CH_2OH + O^{2-} + O_2 \rightarrow CH_2O + O_2^- + OH^-$) and proton accommodation on the surface O^{2-} centers take place already at 77 K, with an apparent activation energy of 8 ± 2 kJ/mol (Fig. 5c). At 293 K the resultant superoxide disappears gradually with the elapsing time, due to its disproportionation into O_2 and O_2^{2} (Fig. 5d).

The EPR parameters of the resultant O_2^- (g_z = 2.0167, g_y = 2.010, g_x = 2.0034) are typical for superoxide trapped on silica, implying that spillover of the hydroxymethyl intermediate from the molybdenum coordination sphere into the silica support takes place. This mechanism is consistent with the observed Mo dispersion sensitivity of methanol oxidation. Application of EPR distinguishes elementary steps that occur within the coordination sphere of the Mo active sites with participation of the adjacent O^{2-} anions, from those which occur on the support surface [101].

4.4. Solid -liquid systems

4.4.1. Reactivity of photogenerated ROS

The nature of principal reactive oxygen species that may be produced on the surface of UV–vis irradiated semiconductor catalysts depends on the pH of the environment [102].

$$O^{2-}{}_{surf} + h^+{}_{VB} \rightarrow O^-{}_{surf}\ pH < pH_{pzc} \quad (7)$$

$$OH^-{}_{surf} + h^+{}_{VB} \rightarrow OH^\bullet\ pH > pH_{pzc} \quad (8)$$

$$O_{2(ads)} + e^-{}_{CB} \rightarrow O_2{}^-{}_{ads} \quad (9)$$

The O_2^- can be transformed into the congener HO_2 radical via protonation reaction $\cdot O_2^- + H^+ \rightleftarrows HO_2$, with pK_a = 4.8, which has a significant impact on the reactivity [103]. The highly oxidizing h^+_{VB} centers, chemically tantamount with the surface O^-_{surf}, may initiate interfacial hole (charge) transfer processes, while interacting with inorganic (e.g., an ubiquitous water) and organic molecules, providing that alignment of the relevant redox potentials is favorable. The hole transfer is often accompanied by proton release.

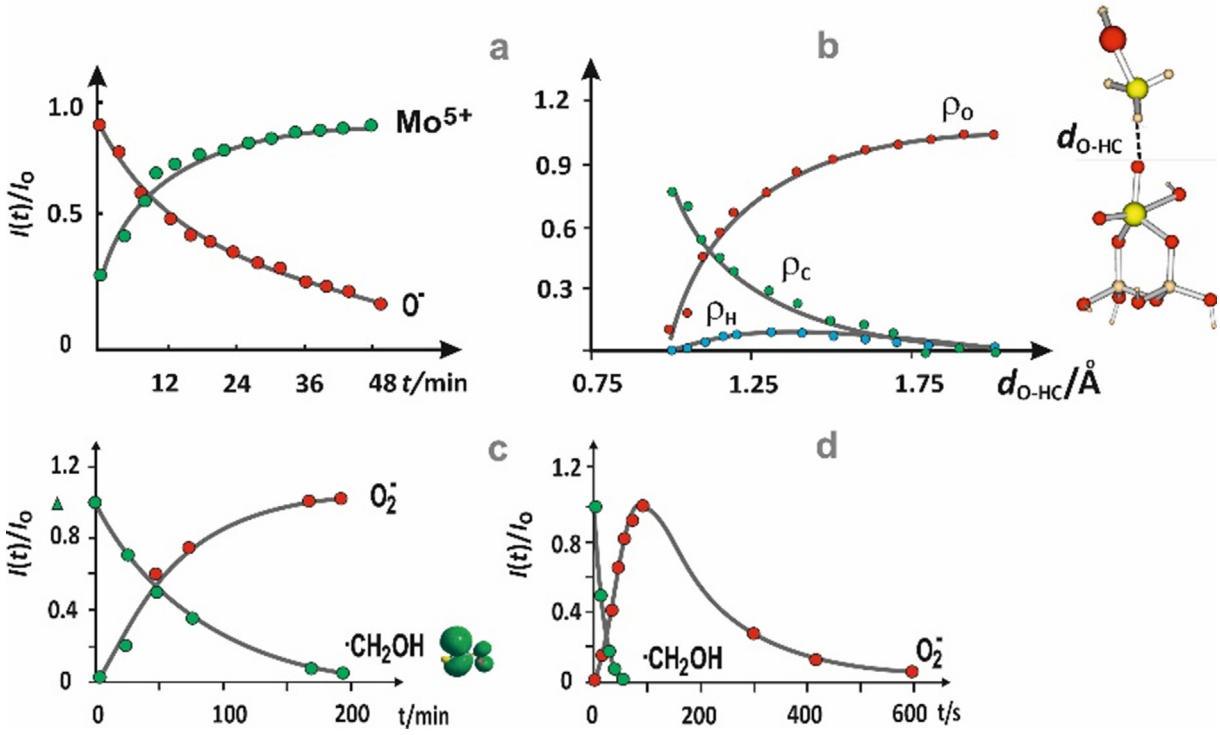

Fig. 5. Kinetic profiles derived from EPR measurements for (a) interaction of O^- with CH_3OH at 210 K, (b) variation of spin density on oxygen, carbon and hydrogen atoms during H-atom abstraction from CH_3OH molecule by the O^-adspecies, and reaction of $\cdot CH_2OH$ with O_2 at 77 K (c) and 293 K (d). Adapted from Refs. [20] and [60].

$$H_2O + O^-_{surf}(h^+_{VB}) \rightarrow \cdot OH + OH^-_{surf} \quad (10)$$

$$R{-}H + O^-_{surf}(h^+_{VB}) \rightarrow \cdot[R{-}H]^+ + O^{2-}_{surf} \text{ or } R{-}H + O^-_{surf}(h^+_{VB}) \rightarrow \cdot R + OH^-_{surf} \quad (11)$$

However, incorporation of surface oxygen $O^-_{surf}(h^+_{VB})$ into the products, proved by isotopic labelling, has also been observed, e.g., in an anoxic oxidation of benzene over titania in the anatase polymorph (with the PZC value of ~ 6) [102].

$$\cdot[R{-}H]^+ + {}^{18}O^-_{surf}(h^+_{VB}) \rightarrow R{-}{}^{18}OH + V^{\cdot\cdot}_{O surf} \quad (12)$$

where $V^{\cdot\cdot}_{O\ surf}$ stands for the generated surface oxygen vacancy. The latter is readily filled with OH species upon dissociative adsorption of a solvent H_2O molecule, making the whole oxidation mechanism reminiscent to the Mars van Krevelen scheme, widely involved in heterogeneous oxidation catalysis [6–8].

In aqueous solutions, localization of the hole on the organic component promotes an immediate reaction of the resultant carbocationic radicals with water either in its molecular or dissociative OH^- form, leading in the case of aromatic compounds to their facile hydroxylation ($\cdot[R{-}H]^+ + OH^- \rightarrow R - OH + H^\cdot$). Such autogenous photohydroxylation fosters utilization of the visible light via the HOMO → CB electron transfer pathway, and is relevant for photocatalytic degradation of those organic pollutants containing aromatic rings that originally do not possess hydroxyl functionalities that are beneficial for visible light harvesting [104]. In aerobic conditions, $\cdot R$ radicals, in turn, react with dioxygen to produce peroxo radicals $ROO^\cdot$. This reaction proceeds usually very rapidly, as implied by the large bimolecular rate constants ($>10^9\ M^{-1}\ s^{-1}$), reported elsewhere [105].

The photogenerated $O^-_{surf}(h^+_{VB})$ ROS are also efficiently reacting with alcohols. It is presumed that oxidation of an exemplary methanol molecule proceeds in two steps: $CH_3OH \rightarrow CH_2OH \rightarrow CH_2O$. It involves the C – H bond cleavage and formation of the corresponding α-hydroxyalkyl radical. Next the aldehyde molecule is produced upon proton release coupled with injection of the electron back into the titania photocatalyst [25]. Such mechanism remains in full analogy with that proposed for an akin gas phase oxidation of CH_3OH over Mo_x/SiO_2 catalyst [100].

The lifetime of the photogenerated $\cdot O_2^-$ in an aqueous environment is one of the longest among ROS species. In the absence of reactants, the superoxide radicals turn into H_2O_2 via disproportionation reaction: $\cdot O_2^- + \cdot HO_2 + H_2O \rightarrow H_2O_2 + O_2 + OH^-$ [106], with the apparent rate constant $k_{obs} = 6 \times 10^{12-pH}\ M^{-1}\ s^-$, which shows pronounced pH-dependence [107]. Such reaction is analogous to O_2^- decay via a disproportionation reaction observed on catalytic oxide surfaces [20]. Reactivity of O_2^- with other molecules in aqueous media is generally rather low in comparison to the $\cdot OH$ radicals, with exception of hydroquinone molecules, where it approaches the diffusion controlled rate ($k \sim 10^{10}\ M^{-1}\ s^-$) [107]. In the case of interaction with molecules of high electron affinity such as ozone, the SIET mechanism prevails ($O_2^- + O_3 \rightarrow O_3^- + O_2$). Reactions of O_2^- with organic compounds are generally initiated by the hydrogen abstraction step: $RH_2 + O_2^- \rightarrow \cdot RH + HO_2^-$ or $RH + O_2^- \rightarrow \cdot R^- + HO_2^-$. Their kinetics is dramatically altered by protonation or deprotonation of both the O_2^- radical and the reactant molecules [103].

4.4.2. Reactivity of ROS derived from H_2O_2

Hydrogen peroxide interacting with oxide surfaces is a common source of reactive oxygen species [108], which are frequently implicated in the heterogenous liquid phase catalytic oxidation processes, with a paramount case provided by the titanium silicate catalysts [109,110]. Other representative catalysts used for H_2O_2 oxidation reactions include metallosilicate T-MCM-41 materials (T = V, Nb, Ti, Cu, Fe, Cr) [111], amorphous oxides of high valent (d^0) metals (ZrO_2, Nb_2O_5, Ta_2O_5) [32,112] and spinels [113]. Three oxidation mechanisms of organic molecules, which are proposed to prevail in such reactions include (i) homolytic pathway where cleavage of the O–O bond in hydrogen peroxide gives rise to $\cdot OH$ radical intermediates engaged in oxygen transfer process, (ii) heterolytic pathway with peroxometallic species as an active oxidant, and (iii) oxo-metal pathway [111].

In the case of amorphous ZrO_2 (PZC = 4.1), Nb_2O_5(PZC = 2.9), or Ta_2O_5 (PZC = 2.3) oxides, an electroprotic mechanism of ROS formation where the $H_2O_2 + HO_2^- = \cdot OH + O_2^- + H_2O$ equilibrium plays a central role has been advanced [32]. Depending on the pH of the reaction mixture various oxygen intermediates such as superoxide (O_2^-) and hydroxyl ($\cdot OH$) radicals as well as peroxide (O_2^{2-}) species were identified. The superoxide and hydroxyl radicals were generated simultaneously in large amounts with the maximum being reached at the pH values around the isoelectric point of the examined oxide gel catalyst. Amorphous state of the oxide catalysts plays the crucial role in this mechanism, since gels act as a sponge for trapping O_2^- and O_2^{2-}, controlling the electroprotic equilibrium. In the particular case of the ZrO_2 gel at pH < 5.3 the catalyst exhibits peroxidase-type activity, whereas at pH > 5.3 formation of the O_2^{2-} species is accompanied by a substantial release of O_2 due to its pronounced catalase-like activity. As a result such oxide gel catalysts, exhibit pH-switchable catalase or peroxidase-like behavior, and were successfully used for oxidation of glycerol and cyclohexene with H_2O_2 [112].

5. O^{2-} Ions - coordination and photoluminescence (PL) studies

As described above, the interaction between monochromatic light and oxide anions can produce paramagnetic oxygen species that can be identified by EPR. The charge transfer between the bare oxide anion, or its protonated form (OH^-), and the metallic cation involved in this activation strongly depends on the coordination and location of both partners. This light absorption produces an exciton that can either deactivate by direct light emission, by a non radiative process or by transferring its energy to another species. Studying these phenomena, by recording the excitation and emission spectra of a given material, PL spectroscopy, offers a unique tool to investigate intrafacial oxide (or hydroxide) environment that exhibit different signals from the equivalent bulk materials [3,4,114,115]. This technique is perfectly complementary to EPR for non-paramagnetic oxygen species characterisation. Moreover, the charge transfer property directly linked to the electron donor ability of the oxide anion is also used to probe the coordination state of the metallic cation. PL also enables following the first steps of photochemical reactions affording a very interesting tool to identify the surface sites involved in the activation step [3,4,114,115].

5.1. Oxide ion coordination in alkaline earth oxides materials

The surface O^{2-} ion located in a position of low coordination (L_C) have been considered to show unusual electron donor properties. However, such surface O^{2-} ions have been difficult to study since they are buried in countless oxide ions and not easily distinguished from those of the bulk. The surface oxide ions on the MgO (1 0 0) plane are described as O^{2-}_{Lc}, with a coordination of 5 or O^{2-}_{5c}, whereas L_C takes the value of 5, 4, or 3 for the different coordination (Fig. 6a). Because of their reduced coordination, their absorption energies are much lower than that of the bulk bands and leads to their different reactivity in catalysis [3,116].

A charge-transfer process produces an exciton, the absorption bands being observed at 160 nm (7.68 eV) and 182 nm (6.8 eV) for pure bulk MgO and CaO, respectively. The excitation of bulk catalyst leading to free excitons undergo a non-radiative thermal decay into phonons, while the excitation of the surface results in a radiative decay of photons (photoluminescence, PL) [3,116]. Thus, different from bulk oxides such as MgO, we could observe the PL spectrum of powdered MgO catalysts outgassed thoroughly to remove surface impurities and hydroxide species at around 350 nm regions when it was excited at around 250 nm region. The peak position (λ_{max}) and yields of PL strongly depended on the outgassing temperature. These results clearly showed that the intrinsic surface sites appearing upon removal of the surface OH^- groups associated with the PL observed with well-outgassed powdered MgO catalysts [116]. There have been many reports to show that such surface site with much lower coordination numbers plays an important role in catalytic reaction as active sites

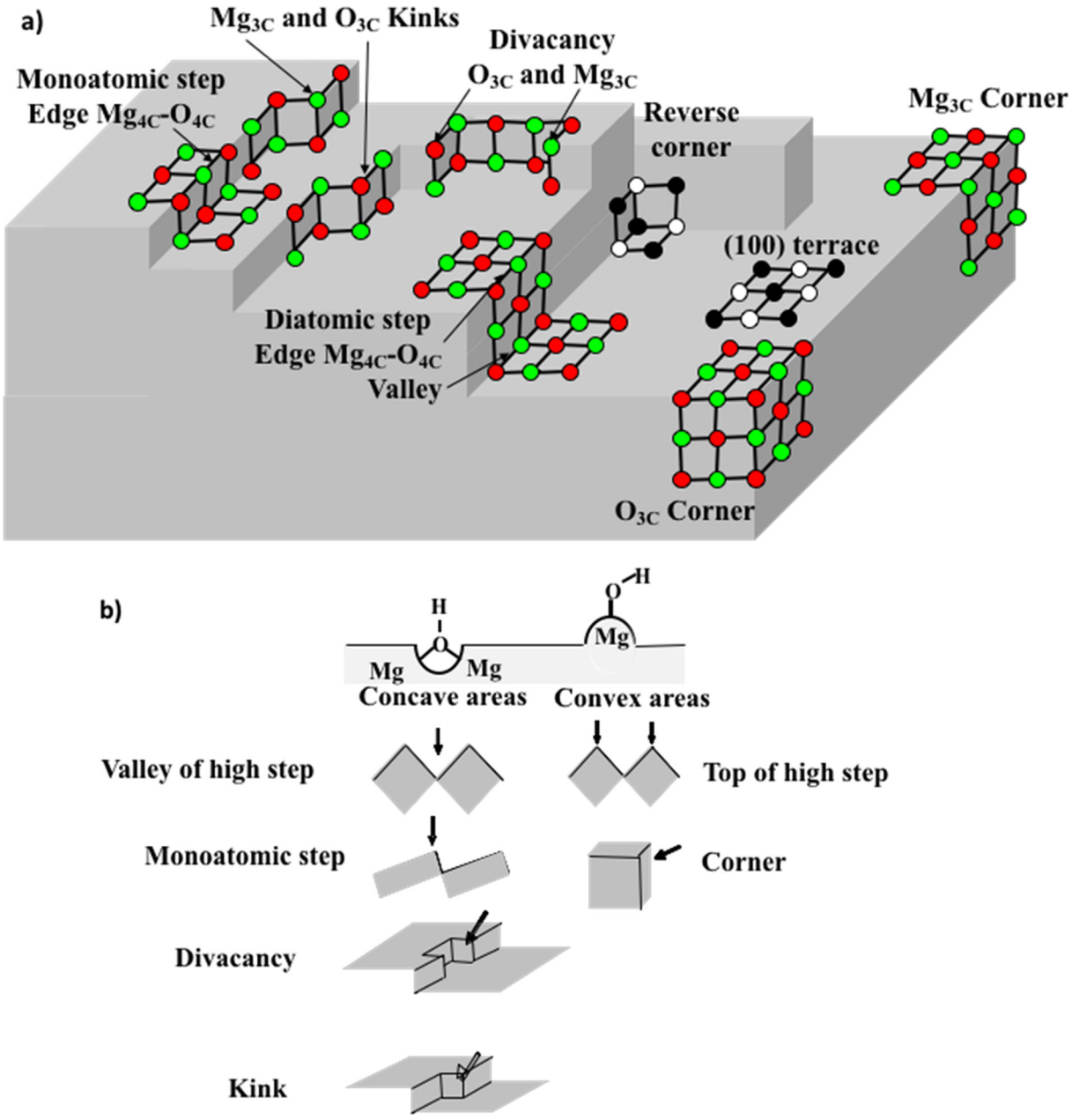

Fig. 6. a) Schematic representation of irregularities on the MgO surface, adapted from [117]. Red circles represent O^{2-}_{Lc} ions and the green circles give the position of Mg^{2+}_{Lc} cations. b) Identification of concave and convex defects, adapted from [118].

for various kinds of reactions such as the isomerization of olefins, cracking reactions, and hydrogenation reactions on the alkaline earth oxide catalysts such as MgO, CaO, etc. [3,116].

This technique has been applied by Che et al. in the 2000's to obtain the fingerprint of alkaline earth oxides samples as model materials of basic catalysts. A coupling to a dynamic vacuum system, first, gave better-resolved and more stable PL spectra in time avoiding quenching phenomena [119]. In a pseudo quantitative approach, the relative distribution of the oxide ions of low coordination O^{2-}_{Lc} was determined and correlated with the shape and size of different MgO and CaO particles determined by TEM and XRD [120,121]. Moreover, PL decay studies of emitting species on MgO nanocubes at room temperature evidenced the energy transfer between excited edge O^{2-}_{4c}, and corner O^{2-}_{3c} [122]. It also exhibited the distinction between kinks and corners by evaluating their PL life times and ability of the emitting species to be formed by energy transfer from excited O^{2-}_{4c}. Combined theoretical and experimental approaches performed at 77 K so as to minimize the energy transfer along the surface, showed that the excitation energy depends not only on the coordination of surface ions, but also on the local topology (kinks *vs* corners for example) and enabled to rationalize the assignment of the experimental PL spectra [123].

5.2. In situ PL studies of oxide semiconducting photocatalytic materials

Titanium dioxide is one of the most popular and well investigated semiconducting photocatalytic materials. The PL spectrum of powdered TiO_2 was observed in a visible light region (λ_{max} at around 500 nm) under the excitation by UV light at around 300 nm, being well understood as a radiative recombination of the photo-formed electrons in the conduction band (CB) and holes in the valence band (VB) at the surface [3,124]. The yields (intensity) of PL changed by the addition of various kinds of gaseous molecules. The yields of PL decreased by the addition of O_2, its extent depending on the amounts of O_2. After sufficient decrease in the PL (quenching), its intensity recovered only partially upon evacuation of the sample at 298 K. EPR measurements of the evacuated sample indicated the formation, in these conditions, of O^-_2 anion radicals adsorbed on Ti^{4+} sites and showed that the irreversible quenching of the PL was due to the formation of O^-_2 at the surface. The addition of N_2O also quenched the PL and showed that small amounts of N_2O simultaneously decomposed into N_2 and O^-. Thus, the formation of negative adducts such as O^-_2 and N_2O^- on the surface by electron transfer from TiO_2 to O_2 or N_2O molecules was found to closely associate with a decrease in intensity of PL (quenching) [3,125].

The presence of a small amount of Pt particles on TiO_2 semiconducting catalysts has been known to lead a dramatically increase in the yield of photocatalytic reaction. Furube et al. investigated the dynamics of charge separation of the photo-formed electrons and holes in TiO_2 and Pt-loaded TiO_2 (Pt/TiO_2) photocatalysts in the whole visible region using a femtosecond diffuse reflectance spectroscopy [3,126]. They found that the fast decay of 4–5 picoseconds in the transient absorption at around 600 nm on Pt/TiO_2 (but not observed on TiO_2) was more rapid with increasing Pt loading for Pt/TiO_2. These dynamic measurements clearly indicated the migration of photo-formed electrons from TiO_2 to Pt nanoparticles, its extent depending on the amount of Pt. Such efficient charge separation of the photo-formed electrons and holes in Pt/TiO_2 photocatalyst was found to closely relate to the efficient photocatalytic reaction on Pt/TiO_2 [3,126].

5.3. In situ PL studies of photocatalytic reactions on metal oxide single site heterogeneous catalysts

Transition metal oxides such as Ti- [127,128], Cu- [129–131] and V-oxide [132–135] single site heterogeneous catalysts have been widely constructed in various types of porous materials such as zeolite and also immobilized on various inert oxide supports such as silica. Detailed characterization studies have been carried out at the molecular level by applying various spectroscopies such as UV–Vis, FT-IR and Raman, ESR, XAFS (XANES and FT-EXAFS) and PL spectroscopies. The electron donating power of the oxide ion is responsible for the formation of a charge transfer excited state of the metal-oxide single site, detected by PL spectroscopy. This behaviour affords both the characterisation of the metal –oxide site and sheds light on the reactivity mechanisms.

5.3.1. Ti-oxide single site heterogeneous catalysts

The XANES (A-D) and FT-EXAFS spectra (a-d) of Ti-Beta(OH), Ti-Beta(F), Ti-HMS and Ti-MCM-41 were measured [127]. The curve-fitting analyses of these XANES spectra clearly indicated the presence of the 4-coordinated Ti-oxide single site species having Ti-O bond length of about 1.84–1.86 Å. These Ti-oxide single site catalysts exhibited the absorption spectrum at 200–280 nm regions with λ_{max} at around 230 nm with subsequent PL at 400–620 nm regions with λ_{max} at around 495 nm. The addition of CO_2 onto these Ti-oxide single site species led to the efficient quenching of the yield and lifetime of the PL. These absorption and PL spectrum of Ti-oxide single site catalysts, together with the results obtained from the FT-EXAFS analyses, clearly indicated that the absorption and PL spectrum were attributed to the charge transfer processes of the 4-coordinated Ti-oxide single site to form its charge transfer excited state and the radiative decay from the charge transfer excited state to its ground state, respectively, as shown in Scheme 2 [3,4 127,128].

It was found that the charge transfer excited state of the Ti-oxide single site species played an important role in various specific photocatalytic reactions which were not found on the bulk semiconducting TiO_2 photocatalysts, suggesting its unique photocatalytic reactivity, being quite different from the bulk semiconducting photocatalysts [3,4 127,128].

5.3.2. Cu(I)/ZSM-5 heterogeneous catalysts

Ion-exchanged copper/zeolite catalysts such as Cu^{2+}/ZSM-5 have been attracted a great deal of attention as potential catalysts for direct decomposition of NOx into N_2 and O_2. On the other hand, Anpo et al. found that the partially reduced copper/zeolite catalysts such as Cu^+/ZSM-5 operate as an effective photocatalyst for the direct decomposition of NOx (NO and N_2O) stoichiometrically into N_2 and O_2 at 275 K. These results clearly suggested that partially reduced Cu^+ species play a significant role as active species in the catalytic and photocatalytic decomposition of NOx into N_2 and O_2 [3,4,129–131].

As shown in the inserted fig. (A) and (C)(a and a′) in Fig. 7, EPR and XAFS (XANES and FT-EXAFS) studies of the Cu^{2+}/ZSM-5 sample indicated that the presence of distorted hydrated Cu^{2+} ions in the C^{2+}/ZSM-5. While, as shown in the inserted fig. (C)(b and b′), the Cu^+/ZSM-5 catalyst prepared by the evacuation of the original Cu^{2+}/ZSM-5 at 973 K exhibits a very strong and sharp band B due to the 1s-4p_z transition, suggesting the Cu^+ ions with a planar 3-coordinate or linear 2-coordinate geometry. As shown in the inserted fig. (B), with Cu^+/ZSM-5 evacuated at temperature higher than 673 K, PL became observable upon the excitation around 300 nm. As shown in the inserted fig. (D), the excitation spectrum of PL (absorption spectrum) having λ_{max} around 290 nm and PL spectrum having λ_{max} at around 450 nm

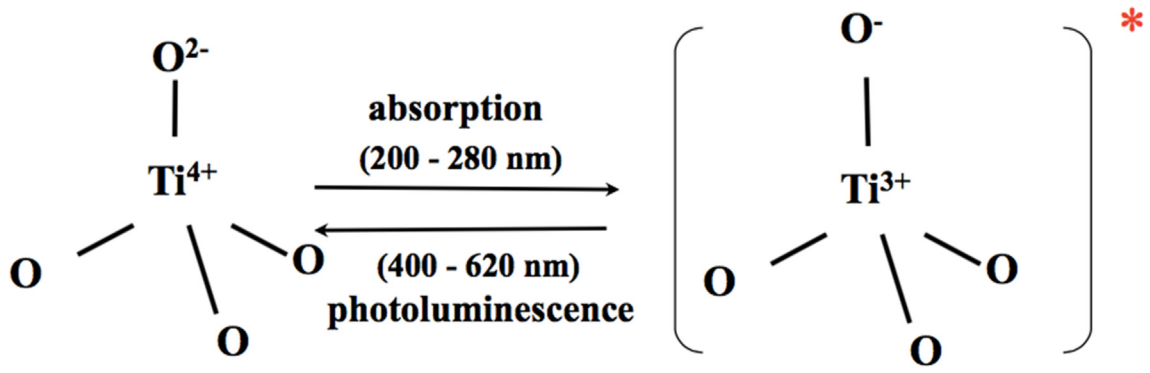

Scheme 2. Charge transfer absorption process at the ground state of the Ti-oxide single site and PL process as a radiative decay from the charge transfer excited state to its ground state.

have been attributed to the excitation $3d^{10} \rightarrow 3d^9 4s^1$ and its reverse radiative deactivation, $3d^9 4s^1 \rightarrow 3d^{10}$ of Cu^+, respectively. The addition of NO onto the Cu^+/ZSM-5 was found to lead an efficient quenching of the PL. The lifetime of the PL was also found to shorten by the addition of NO with increasing the pressure of added NO. The evacuation of the system after the quenching led the complete recovery of the PL to its original intensity and lifetime. As shown in the inserted fig. (E) and (F), both FT-IR spectra and EPR signal observed in the presence of NO exhibit the presence of nitrosylic adducts, $(Cu\text{--}NO)^+$ as the major adsorbed species. UV irradiation of the Cu^+/ZSM-5 with $(Cu\text{--}NO)^+$ species led to a decrease in the intensity of the FT-IR spectra and EPR signal due to $(Cu\text{--}NO)^+$ with irradiation time. After the UV irradiation was stopped, the intensities on the EPR signal and FT-IR spectrum returned to their original levels, suggesting that not only that $(C\text{--}NO)^+$ species act as reaction precursors but also that the photoinduced decomposition of NO proceeds catalytically [129–131,136].

Fig. 7 summarizes these experimental results together with the proposed reaction mechanism for the photocatalytic decomposition of NO into N_2 and O_2 on the Cu^+/ZSM-5 catalyst under UV light irradiation at 275 K. It is expected that an electron transfer from the excited state of the Cu^+ ion ($3d^9 4s^1$ state) to the π-antibonding orbital of NO and simultaneous an electron transfer from the π-bonding orbital of another NO to the vacant electron state of the Cu^+ ion ($3d^9 4s^0$ state) occur, causing local charge separation and weakening of the N-O bond of 2 NO molecules at a Cu^+ site that resulting in the selective formation of N_2 and O_2 without any formation of N_2O and/or NO_2 [129–131,136].

5.3.3. V-oxide single site heterogeneous catalysts

The photoluminescence spectrum is well defined but it is also often partially resolved or even unresolved. This can be explained by the molecular electronic transition which does not always correspond to a well-defined quantum of energy because different nuclear geometries are associated with the initial or final electronic energy states, leading to partially resolved or unresolved spectra. Such a situation is most likely found for molecules in solution. In certain cases, however, some vibrational fine structure is observed in the PL spectrum of highly dispersed metal-oxide single site heterogeneous catalysts. These prominent vibrational fine structures are associated with the fact that the nuclear equilibrium positions of the oxide catalysts are most dramatically changed by the radiative electronic transition [3,4,132,133].

The data obtained by IR, UV–Vis. and ^{51}V NMR showed that vanadium was present as tetrahedral V^{5+} ions. However, despite the combined development of those techniques, it was difficult to conclude whether in V-loaded β-zeolite there was a single or several kinds of tetrahedral V^{5+} species. On the basis of PL spectra, Dzwigaj et al. distinguished three kinds of tetrahedral V^{5+} species (α, β, γ) in VSiβ zeolite with 1.5 V wt%. They also showed that their relative concentrations strongly depended on dehydration/rehydration treatments [4,134,135]. They found that C-Hyd-VSiβ zeolite exhibited PL spectra with λ_{max} at around 500 nm showing a complex vibrational fine structure [134,135]. Those spectra corresponded to radiative transitions from the lowest vibrational energy level of the charge transfer excited state $(V^{4+} - O^-)^*$ of tetrahedral coordinated O = VO_3 units to the various vibrational energy levels of its ground state $(V^{5+} - O^{2-})$.

In order to ease the analysis of the very complex spectra due to the superimposition of different vibrational fine structures, the second-derivative PL spectra were measured. The energy separation between the $(0 \rightarrow 0)$ and $(0 \rightarrow 1)$ vibrational transitions were determined from the second derivative PL spectrum, and the vibrational energies were found to be equal to 1018 cm^{-1} for α species, 1054 cm^{-1} for β species and 1036 cm^{-1} for γ species, in good agreement with the vibrational energy for V=O bond obtained by IR and Raman measurements for gaseous $O{=}VF_3$, liquid $O{=}VCl_3$ and $O{=}VBr_3$ molecular compounds as well as various supported vanadium oxide catalysts (V-oxide/SiO_2, V-oxide/PVG, and V-oxide/γ-Al_2O_3, V-oxide/β-zeolite, where PVG stands for porous Vycor glass) [3,4,132–135]).

The photocatalytic oxidation of CO with N_2O to form CO_2 and N_2 was found to proceed with a good stoichiometry on the highly dispersed V-oxide single site heterogeneous catalyst constructed within the frameworks of MCM-41. From the analyses of XANES and FT-EXAFS, V-oxide species was found to have one short V-O bond of 1.61 Å and three long V-O bonds of 1.79 Å. In the charge transfer excited state, the V-O bond of the V=O (vanadyl) group was found to become longer and weaker, easily reacting with CO to form CO_2 and reduced V^{3+} species [132,133]. The PL of V-oxide single site catalyst and its quenching by the addition of CO indicated that CO easily interacted with the charge transfer excited state of V-oxide with some irreversible quenching even after evacuation of CO. FT-IR spectra of CO clearly indicated that CO adsorbed on the reduced V^{3+} species at around 2167 and 2183 cm^{-1} and then its species disappeared by the addition of N_2O onto the catalyst. These results clearly suggested that under UV light irradiation in the presence of CO, V^{4+} species easily reacted with CO to form V^{3+} and CO_2 with subsequent adsorption of CO molecules onto V^{3+} species, and then, thus formed V^{3+} species was easily re-oxidized into V^{5+} species by N_2O molecules in the system. From these results, the reaction mechanism for the photocatalytic oxidation of CO with N_2O to form CO_2 and N_2 was proposed [3,4,132,133].

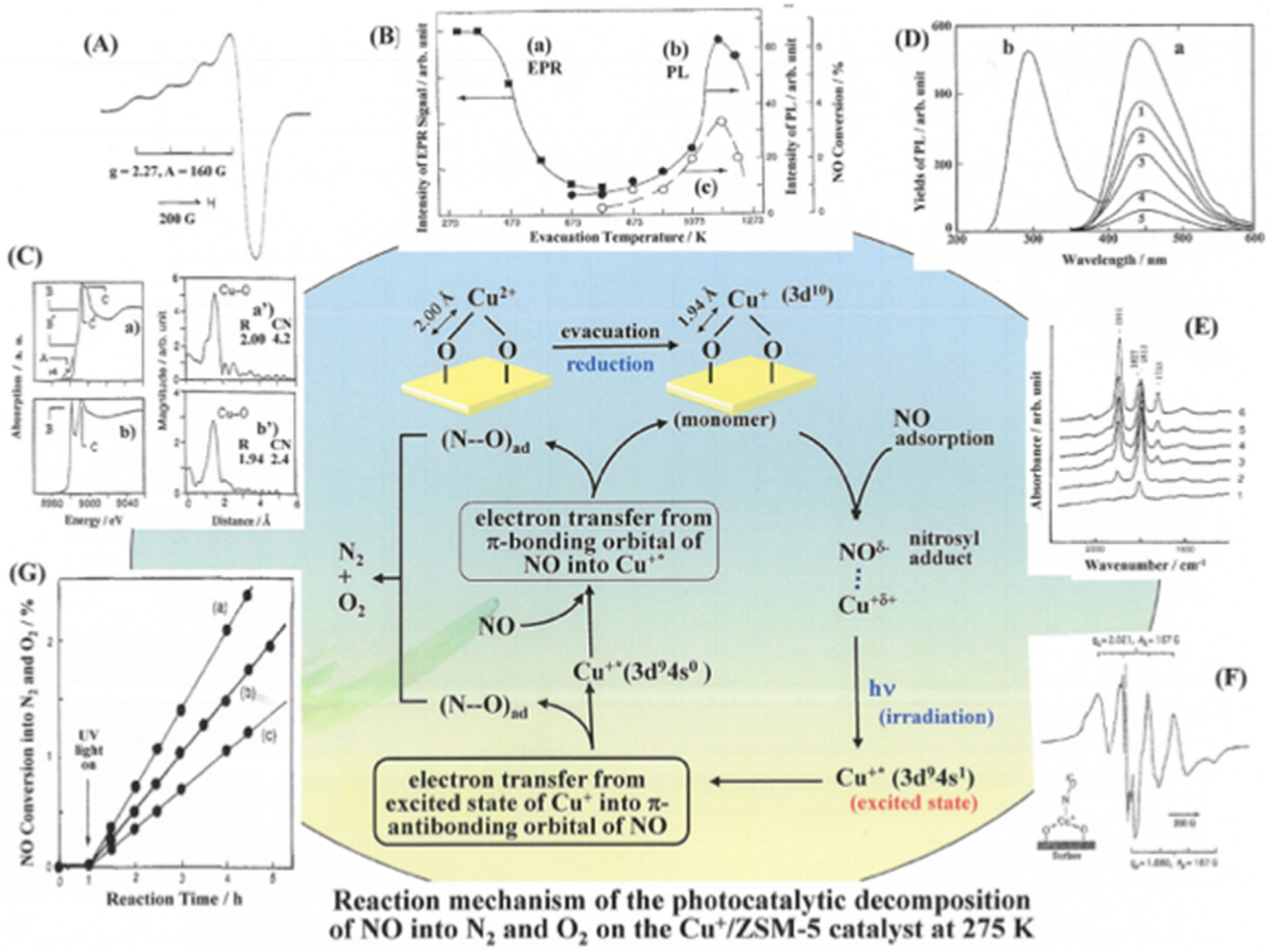

Fig. 7. Proposed reaction mechanism for the photocatalytic decomposition of NO into N_2 and O_2 on Cu^+/ZSM-5 catalyst at 275 K. Inserted fig. (A) is EPR spectrum of the Cu^{2+}/ZSM-5 sample evacuated at 373 K (EPR signal recorded at 285 K). Inserted fig. (B) shows the effects of the evacuation temperature of the Cu^{2+}/ZSM-5 sample on the relative intensity of the EPR signal due to Cu^{2+} (a), the relative yields of the PL due to Cu^+ (b), and the relative conversion (yields) of the photocatalytic decomposition of NO at 275 K (c). Inserted fig. (C) shows XANES (a), b)) and FT-EXAFS (a′) and b′)) spectra of the (a) and b)) Cu^{2+}/ZSM-5 sample and the (b) and b′)) Cu^+/ZSM-5 catalyst prepared by evacuation of the original Cu^{2+}/ZSM-5 sample at 973 K. Inserted fig. (D) shows the effect of the addition of NO at 293 K on the PL spectrum of the Cu^+/ZSM-5 catalyst prepared by the evacuation of the Cu^{2+}/ZSM-5 sample at 1173 K. The addition of NO was carried out at 295 K. NO pressure (in Torr): 1; 0.1, 2; 0.3, 3; 0.5, 4; 1.5, 5; 20. The excitation spectrum (b) was monitored at 450 nm emission of (a). Inserted fig. (E) shows FT-IR spectra of NO species adsorbed onto the Cu^+/ZSM-5 catalyst prepared by the evacuation of the Cu^{2+}/ZSM-5 sample at 1173 K. The adsorption of NO was carried out at 290 K. NO pressure (in Torr): 1; 0.1, 2; 2.0, 3; 3.0, 4; 5.0, 5; 10, 6; 20. The spectra were recorded at 298 K. Inserted fig. (F) shows EPR spectrum of NO species (nitrosyl adducts) adsorbed onto the Cu^+/ZSM-5 catalyst prepared by the evacuation of the Cu^{2+}/ZSM-5 sample at 1173 K. EPR spectrum was recorded at 77 K. Inserted fig. (G) shows reaction profiles of the photocatalytic decomposition of NO into N_2 and O_2 at 275 K on the Cu^+/ZSM-5 (a), Cu^+/Y-zeolite (b), and Cu^+/SiO_2 catalyst (c), respectively. No reaction was observed at 275 K without UV light irradiation.

In addition to these single site heterogeneous catalysts, the PL studies have been reported with other various kinds of metal-oxide single site heterogeneous catalysts constructed in zeolites [3,135] and Metal-Organic Frameworks (MOF) [137]. Furthermore, currently, the PL studies have been widely utilized to characterize the various kinds of catalysts not only metal-oxide catalysts but also metal-complexes anchored on mesoporous silica [138]. Thus, the PL studies combined with other physicochemical techniques and spectroscopies provide us very useful information for rational design and development of highly functional heterogeneous catalysts and photocatalysts.

6. O^{2-}_{Lc} ions and their basicity

As already discussed, surface oxide anions, depending on the metal-oxide system, may exhibit a strong electron donating power that can lead, upon light absorption, to excited and reactive metal-oxide species (Section 5). It may also deprotonate organic molecules and the carbanion thus formed may further react in an oxidative medium (Section 4.3). But, this basicity can also lead directly to further transformations of organic molecules as very well known in homogeneous catalysis. Despite an initial limited use of solid bases in industry [139] their interest has been growing since the 1970s [140]. Their applications, ranging from alkene isomerization to fine chemistry, have been reviewed [141–143] and more recently, because of the major interest in converting biomass sourced platform molecules, new materials and new reactions involving surface sites able to deprotonate a molecule have been studied [144–146]. The role of base sites as a key parameter in already known reactions is also underlined in very recent reviews [147–152].

The link between the electron donating ability of oxide ions and their basicity was quite early questioned in the community as shown in Che and Tench 82's review article [1]. In line with the original Brønsted's definition [153], in 2001, Hattori [142] considered the basic properties of an inorganic material as the ability to deprotonate an organic molecule and pointed out also the crucial role of acid-base pairs. Most of the studies [141,142,154] aiming to characterize the basic properties of a surface used the adsorption of non protic probe molecules (like carbon dioxide or sulfur dioxide) followed by spectroscopy [155], by thermodesorption techniques [156] or modelled [157] but this approach sometimes failed to account for the tendencies observed in basic catalytic reactions. This discrepancy between CO_2 TPD and the true ability of a surface to deprotonate an organic molecule has been still recently underlined by Davis et al. [152] or by Weckhuysen et al. [158]. In an original way, the question of the link between the ability of the surface to share an electron pair, hence its Lewis basicity, and to deprotonate a molecule, hence its Brønsted basicity, was raised in the group of Michel Che.

6.1. Model studies on alkaline earth oxides

Magnesium oxide (extended to calcium oxide), well-known basic catalyst, was thus chosen as a model system and characterized by means of concomitant use of protic probe molecules adsorption followed by IR, photoluminescence and NMR spectroscopies, coupled with DFT calculations, and correlated with the catalytic behaviour in the 2-methyl-but-3-yne-2-ol (MBOH) model reaction [159].

Different preparation routes have been used to vary the relative distribution of O^{2-}_{Lc} ions. The materials were systematically treated under vacuum at 1273 K to control the desorption of the classical contaminants of MgO surfaces (water and carbon dioxide) (and thus the availability of bare oxides ions) and to further avoid the sintering of the surface upon thermal treatments as described in former studies [142]. The controlled rehydroxylation [160] or recarbonation [161] of the surface were performed to evaluate how these natural "contaminants" of basic oxides, still present in most studies performed at moderate temperature, impact the basicity of a given surface.

6.1.1. Evaluation of MgO Brønsted basicity.

The protonation of O^{2-}_{Lc} generates $O_{Lc}H^-$ groups, which formation can be monitored by photoluminescence, IR and NMR. To help their identification, hydroxylation of MgO surfaces was first investigated [118] in a preliminary work, by DFT simulation of the hydration of $Mg^{2+}_{Lc}O^{2-}_{Lc}$ pairs and determining the thermodynamic stabilities of the resulting surfaces [162].

Controlled hydroxylated surfaces formed upon the adsorption of water or methanol were followed by PL spectroscopy and three PL species were assigned to surface OH groups [120]. TD-DFT excitation energy calculations performed on hydroxylated MgO clusters [163] indicates that the hydroxylation state of the surface can accurately be followed by the evolution of the bands characteristic of bare surface irregularities. In addition, $O_{Lc}H$ groups are themselves directly involved in the excitation process only if they are located on convex areas of the surface and if $L \leq 3$ (see Fig. 6a).

Unlike previous model proposed for the assignment of IR spectra (isolated OH for narrow band at 3750 cm^{-1} and H-bonded one for broad band at lower wavenumber [164]), this new original model perfectly accounts for the dependence of IR spectra on $O_{Lc}H$ coordination and topology and for their evolution upon thermal treatment. In particular, it is found that there are only very few $O_{Lc}H$ located or corner or kink remaining isolated and it is the hydrogen-bonding type (acceptor *vs* donor) parameter that influences most the IR frequency of OH groups (high and low frequencies, respectively) [162]. This main parameter is followed by the location of $O_{Lc}H$ groups in concave or convex areas of the surface and then oxygen coordination (Fig. 6b). Complex ^1H MAS NMR spectra of hydroxylated MgO powders have also been assigned [165]. The highest chemical shifts ($\delta H > -0.7$ ppm) are assigned to hydrogen-bond donor OH groups (O_{3c}-H, O_{4c}-H and O_{5c}-H). The lowest chemical shifts ($\delta H < -0.7$ ppm) are associated to isolated and hydrogen-bond acceptor O_{2c}-H and O_{1c}-H, whereas the central signal at ($\delta H = -0.7$ ppm would correspond to isolated O_{3c}-H and O_{4c}-H on kinks and divacancies. The assignment is fully consistent with the OH_{Lc} generated upon CD_3OH adsorption [166] and with quantitative analysis of the evolution of spectra with temperature.

Thanks to these spectroscopic tools, the deprotonation ability of MgO surfaces of various morphologies towards protic molecules, such as water [118], propyne and methanol was complementary followed by FTIR [160,167] and photoluminescence [119,167] spectroscopies. The same trend is observed for propyne and methanol: (i) the amount of dissociated species increases with the relative concentration of oxide ions of low coordination O^{2-}_{Lc}, (ii) Mg^{2+}_{Lc} ions are also involved in the deprotonation process. Quantitative adsorption and IR measurements suggest that the deprotonating $Mg^{2+}O^{2-}$ pairs involve 3- and 4- coordinated ions: $Mg^{2+}_{3c}O^{2-}_{4c}$ and $Mg^{2+}_{4c}O^{2-}_{3c}$. They, thus combine a strong Brønsted basic site O^{2-}_{Lc}, able to abstract a proton and a strong acidic Lewis site able to stabilize the anion generated by deprotonation.

Such a determining role of the Lewis acidic site in stabilizing the deprotonated species, thus in increasing the Brønsted basicity, [118] implies a key role played by surface topology. The stabilization of the hydroxyl group formed upon water deprotonation is greatly favoured in concave areas of the surface (bottom of the monatomic step for example, see Fig. 6b) due to the bridging geometry involving two Mg^{2+} cations. It was thus inferred that the deprotonation ability scale of the different defects may also depend on the reactant molecule and on its ability to be stabilized on the surface in its deprotonated form.

In line with this conclusion, a DFT study [161] also shows that the strongest Lewis basic sites (probed by CO_2 adsorption) are different from the strongest Brønsted basic sites (probed by water adsorption), on MgO surface, being identified on the one hand as steps and on the other hand as kinks and divacancies, respectively. Hence, if by nature and definition, all Lewis bases are also Brønsted bases and reciprocally, the strength scale is different depending on the nature of the considered basicity.

6.1.2. Thermodynamic basicity vs kinetic basicity

The relationship between thermodynamic Brønsted basicity and the reactivity of basic sites (kinetic basicity) of MgO samples was investigated [160] comparing results obtained from the equilibrium of deprotonation of a protic molecule and from the MBOH conversion used as a model reaction. Despite a low deprotonation ability, hydroxylated surfaces are more reactive than bare ones. It was shown by ^1H NMR, that discriminates between the $O_{Lc}H$ species that the lowest coordinated $O_{1c}H$ and $O_{2c}H$ base sites formed by water dissociation on steps and corners [168] are responsible for the high catalytic conversion of MBOH of hydroxylated surfaces. According to the simulations of the reaction pathways based on the Nudged Elastic Band (NEB) method [169], a lowering in the activation energy barriers is induced by surface OH groups, providing a bare Mg^{2+}–O^{2-} pair is still available in their vicinity for MBOH to adsorb and react. Thus, OH groups do not directly interact with MBOH reactant but they modify the basic reactivity of the vicinal bare Mg^{2+}–O^{2-} pair on which MBOH adsorbs and converts.

In the case of CaO, such a predominant role played by the remaining hydroxyls left on the surface on the kinetic basicity was confirmed for MBOH, even for pretreatment up to 1023 K [121,170]. In addition, the higher intrinsic basic reactivity of hydroxyl on CaO than on MgO is ascribed i) to the weaker Lewis acid properties of Ca^{2+} than Mg^{2+}, which could make electronic lone pairs of the related OH groups more available to play a role in the mechanism as nucleophile or as efficient acceptor of hydrogen bond and ii) to lower Madelung potential of CaO, that makes the surface ions more likely to geometrically relax upon adsorption of hydroxyl groups and reactive molecule, finally leading to adsorption configuration more favorable to the reactivity of the intermediate.

6.2. Relevance of these concepts in the new challenges of basic catalysis

In 30 years the application field of base catalysts has considerably grown due to the need to valorize bio-sourced molecules. Our purpose is not to review here this large domain but to focus on the way base sites are now described and characterized.

6.2.1. Acid-base pairs and their characterization

The idea that a reaction occurring in basic media in homogeneous catalysis, must find an acid base-pair on the surface of a solid catalyst, to abstract the proton and to stabilize the formed anion, is now very often considered [152,171]. Thus many studies aim to control the acidity of the base catalysts working for example on the nature of the metallic cation in MOF materials to enhance the reactivity in Knoevenagel reaction [172], or incorporating Lewis acids on MgO, for example by thermal decomposition of hydrotalcites, to reach the appropriate acid-base balance as reviewed by Davis et coll. for Guerbet reaction [152].

The less coordinated are the acid and base elements of the pair, the strongest is the deprotonating ability. Defectuous oxide surfaces are thus very interesting in base catalyzed reactions requiring a strong stabilization of the deprotonated species. For hept-1-ene isomerization, it has been shown [173] that a maximum activity was obtained on MgO pretreated at moderate temperature (750 K) without any relation with the evolution of the specific surface area as initially proposed by Hattori [142]. By means of a mixed experimental-theory study of CO_2 adsorption followed by IR spectroscopy, the transient formation of unstable MgO planes as (1 1 1) or (1 1 0) was evidenced in these conditions. The high basic strength of these unstable planes is now well admitted in the literature as shown for example in the case of carbon oxides adsorption [174].

Nevertheless, acid-base pair concept should not be confused with the coexistence on a same material of acidic and basic phases. For example, in the case of MgO-SiO_2 system that was extensively studied for bio-ethanol cascade reaction conversion into butadiene and recently reviewed by Pomalaza et al. [175], it was shown that acidic sites (on silica or on magnesium silicates) are involved in the dehydration steps whereas the basic ones (on MgO) catalyse the dehydrogenation and condensation steps. In this case, the catalyst is bifunctional, the two properties are independently characterized and the optimal balance between acid and base phases is defined.

6.2.2. Role of oxygen vacancies

On the materials that can form oxygen vacancies, the electronic density of base sites can be modified, influencing the catalytic performances. It was shown, for example on ZnO that the pre-treatment temperature or the nature of the atmosphere were decisive to tune its basic reactivity probed in MBOH conversion. Combining EPR and photoluminescence characterizations of the resulting defects [176 177,178], this effect was ascribed to the modulation of electronic density of the active acid-base pair by the electron release or capture associated to the formation (reductive conditions) or filling up (low temperature oxidative conditions) of Vo^{+} oxygen vacancies, respectively [179]. The reaction temperature is also a critical point for the stability of the basic reactivity. When low enough (130 °C for MBOH reaction), DRIFT operando studies shows that the water formed during the reaction dissociates and finally participate to the filling up of oxygen vacancies, killing the strongest basic sites and being thus responsible for reaction deactivation [180]. On the contrary, for ethanol conversion reaction implemented at high temperature enough (350 °C), the rapid desorption of water preserves the oxygen vacancies formed during the high thermal pre-treatment and the beneficial influence of controlled conditions of the pre-treatment can be maintained [179].

Similar phenomenon was recently demonstrated by Chagas et al. [181] in ethanol conversion to butadiene enhanced by Zn doping of ZrO_2 for. The authors show by EPR the replacement of Zr^{4+} by Zn^{2+} in the zirconia lattice leading to the formation of strong acid-base pairs linked to coordinatively Zr^{+}_{4} and oxygen vacancies respectively.

6.2.3. Role of hydroxyl groups

One of the important features of recent work on basic catalysts is the confirmation of the key role often played by hydroxyls groups. Water adsorption/dissociation that was usually considered as a poison of basic reactivity, appears favourable in many cases. The interest of non-calcined double lamellar hydroxides is known for many years but their applications like aldolisation, Knoevenagel or Claisen-Schmidt condensation increased in liquid phase as summarized in a recent review [182]. Moreover, if thermal activation of carbonate containing hydrotalcite led to basic MgAlO mixed oxide, its subsequent rehydration under CO_2 free conditions allows recovering the hydrotalcite structure with an enhanced activity ascribed to the higher density of accessible OH [183].

Recently, the role of molecular water adsorption was for example evidenced on magnesium silicates for transesterification reaction [184] and demonstrated by DFT calculations in the case of aldol condensation on MgO surfaces [185], showing that hydroxyl groups induce a lowering in the activation barriers for the overall reaction. The authors conclude that this kind of reaction, even if considered to occur on basic surfaces, needs a strong Lewis acid site combined with a medium to weak basic site.

6.2.4. Towards a coordination chemistry of anions

From these studies, the conclusion was deduced that the strongest electron donation oxide ion is not necessarily the best basic sites from a thermodynamic point of view. Thus, new research areas merged to investigate the reactivity of other anions in light of their coordination chemistry. To exemplified briefly these ongoing studies, we can focus on the work already made on hydroxyapatite, a biocompatible calcium phosphate with generic formula $Ca_{10}(PO_4)_6(OH)_2$, involving a flexible framework that makes its composition tunable due to substitution ability [186–188] and non-stoichiometric properties [189]. This non-stoichiometry composition was long used to describe the tunable catalytic properties ranging from acidic to basic. To go further than this empirical relationship between bulk composition and

surface reactivity, more accurate surface descriptors were required. H-D isotopic labelling followed monitored by FTIR and ssNMR allowed us to discriminate the spectroscopic fingerprints of bulk and surface OH^- and HPO_4^{2-} [190,191]. If surface OH emerging from channels was clearly identified as the basic site, [192] the key role played by its acidic partner of the acid-base pairs was confirmed for alcohol reactions: i) the conversion linearly increases as the fraction of surface POH/Ca^{2+} probed by CO adsorption increases [193] and ii) from an operando DRIFT study, the involvement of the atypical POH-OH acid-base pair is responsible for the unique selectivity in n-butanol in the ethanol conversion [194].

7. Perspectives and hurdles

Summarizing, EPR spectroscopy is a powerful, non-destructive spectroscopic techniques that is highly sensitive in detection of paramagnetic species. It has been applied successfully in the field of surface chemistry and catalysis related studies, and appears unrivalled while probing active sites nature, radical reaction intermediates and low temperature processes occurring within the coordination sphere of active sites constituted by the transition metal ions. Using dedicated cells, EPR spectroscopy may be used in an operando mode, also in conjunction with other characterization techniques [195]. Owing to large information content of the EPR signals, and their extreme sensitivity to the of electronic structure of the identified paramagnetic active centres and reaction intermediates, extraction of their complex parameters provide valuable constraints for sensible molecular modelling of active sites and catalytic reaction mechanisms.

As described in Sections 3 and 4, EPR has provided essential information on the nature of the surface oxygen species and their reactivity in model and real catalytic reactions. In particular, it is shown that the reactive oxygen species described herein are labile and highly reactive even at relatively low temperatures. For this reason, and to achieve a good spectral resolution, the EPR spectra are usually recorded at temperatures below 100 K, though successful applications up to 500–600 K are also reported [196]. Despite the described inherent limitations, the potential of EPR investigations in heterogeneous catalysis is still growing, thanks to the development of pulse-EPR techniques. The latter allow to resolve very weak magnetic interactions to explore a larger sphere around a given paramagnetic centre, providing essential information both on its local structure and on the chemical bonding with the surroundings and with the reactants, including bond lengths and angles unavailable by other spectroscopic methods [197–199].

The fundamentals of PL spectroscopy and its applications are very important to elucidate the surface coordination sates, surface band structure and surface active site related to adsorption, catalysis and photocatalytic reactions on various bulk oxides such as MgO, inorganic and organic semiconducting catalysts such as TiO_2 and g-C_3N_4, and highly dispersed single-site heterogeneous catalysts such as Ti-oxide, V-oxide, and Cu(I)/ZSM-5 at their working states on the molecular level.

In comparison to other spectroscopic techniques, PL studies have opened the new possibility of directly observation of surface active site including lattice O^{2-} ions located at unsaturated lower coordination states with its high sensitivity and non-destruction. Only PL studies offer insights into their reactivity and dynamics of the excited states of catalysts including to obtain the absolute reaction rate constants of various reactant molecules such as O_2, CO, CO_2, NO and H_2 toward the excited states of catalysts. Dynamic aspects of the in situ PL studies related to the photocatalytic reactions on the bulk semiconducting catalysts and highly dispersed metal oxide single-site heterogeneous catalysts have been focused to show the predominance of PL studies to understand the photocatalytic reaction mechanisms at the molecular level.

PL studies combined with other physicochemical techniques and spectroscopies such as diffuse UV reflectance, FT-IR, EPR, and XAFS are expected to provide us very useful information to rational design and development of highly functional catalysts and photocatalytic materials which are applicable to the production of clean energy and sustainable environment for human beings, especially, by effective and efficient utilization of sunlight which are the most important issues in 21st century.

Due to the development of new applications involving the basic properties of the catalysts, it appears essential to maintain the effort to understand at a molecular level the nature of the sites involved and the mechanism of the reactions. Of course, real catalytic systems are often very complex and exhibit mixture of phases as exemplified by MgO-SiO_2 systems studied for the conversion of ethanol in butadiene. Nevertheless, the use of model systems and of DFT calculations as proposed for example by Taifan et al. [200] for ethanol conversion may help to shed light on the key parameters to be improved for a given reaction.

Basic sites are easily covered by natural acidic pollutants like CO_2 and water that was usually considered as an important drawback as it inhibits the "strongest sites". Nevertheless, it appears finally that the reactivity of a basic site is in many case more linked to the acid-base balance of the pair than to the Lewis strength of the oxide ion. Thus the role of water or hydroxyls groups on the reactivity must systematically be examined and weak/medium bases as carbonates must also be considered.

Last, the new applications of basic catalysts, linked to the valorization of bio-sourced molecules are often processed in liquid phase. To investigate the acido-basic properties of a solid in a liquid medium, Gervasini et coll. developed a set up for the measurement of adsorption isotherms of probe molecules in solution. Such a development of in situ characterization techniques of the solid-liquid interface must be increased [201] to afford a better description of the molecular phenomena occurring in these conditions.

Declaration of Competing Interest

The authors declare that they have no known competing financial interests or personal relationships that could have appeared to influence the work reported in this paper.

Acknowledgements

The co-authors want to warmly thank here all the collaborators who closely work with Michel Che on these subjects. Among them, J. Vedrine, his long term (from PhD in Lyon) friend, C. Louis who participated in a lot of the studies mentioned in this review, F. Averseng, A. Davidson, S. Dzwigaj and J. Fournier researchers in his group in Paris and also the technical staff, B. Morin (EPR engineer at LRS) and R. Franck (Engineer who started PL in LRS). All the PhD students and Post-Docs mentioned in the following references are also warmly acknowledged.

References

[1] M. Che, A.J. Tench, Characterization and reactivity of mononuclear oxygen species on oxide surfaces, Adv. Catal. 31 (1982) 77–133.
[2] M. Che, A.J. Tench, Characterization and reactivity of molecular oxygen species on oxide surfaces, Adv. Catal. 32 (1983) 1–148.
[3] M. Anpo, M. Che, Applications of photoluminescence techniques to the characterization of solid surfaces in relation to adsorption, catalysis, and photocatalysis, Adv. Catal. 44 (1999) 119–257.
[4] M. Anpo, S. Dzwigaj, M. Che, Applications of photoluminescence spectroscopy to the investigation of oxide-containing catalysts in the working state, Adv. Catal. 52 (2009) 1–42.
[5] M. Anpo, M. Takeuchi, K. Ikeue, S. Dohshi, Design and development of titanium oxide photocatalysts operating under visible and UV light irradiation. The applications of metal ion-implantation techniques to semiconducting TiO2 and Ti/zeolite catalysts, Curr. Opin. Solid State Mater. Sci. 6 (2002) 381–388.
[6] A. Bielanski, J. Haber, Chemical Industries, Vol. 43: Oxygen in Catalysis, Marcel Dekker, Inc., 1991.
[7] J.C. Vedrine, I. Fechete, Heterogeneous partial oxidation catalysis on metal oxides, C. R. Chim. 19 (2016) 1203–1225.
[8] B. Grzybowska-Swierkosz, Thirty years in selective oxidation on oxides: what have we learned?, Top. Catal. 11 (12) (2000) 23–42.
[9] S. Kwon, P. Deshlahra, E. Iglesia, Dioxygen activation routes in Mars-van Krevelen redox cycles catalyzed by metal oxides, J. Catal. 364 (2018) 228–247.
[10] M. Che, K. Dyrek, M. Kermarec, A.J. Tench, Characterization of oxygen species adsorbed on oxide surfaces by infrared spectroscopy, Rev. Chim. Miner. 21 (1984) 669–679.
[11] K. Hayashi, S. Matsuishi, N. Ueda, M. Hirano, H. Hosono, Maximum incorporation of oxygen radicals, O- and O2-, into 12CaO·7Al2O3 with a nanoporous structure, Chem. Mater. 15 (2003) 1851–1854.
[12] S. Maurelli, M. Ruszak, S. Witkowski, P. Pietrzyk, M. Chiesa, Z. Sojka, Spectroscopic CW-EPR and HYSCORE investigations of Cu2+ and O2- species in copper doped nanoporous calcium aluminate (12CaO·7Al2O3), Phys. Chem. Chem. Phys. 12 (2010) 10933–10941.
[13] Z. Sojka, Molecular aspects of catalytic reactivity. Application of EPR spectroscopy to studies of the mechanism of heterogeneous catalytic reactions, Catal. Rev. - Sci. Eng. 37 (1995) 461–512.
[14] A. Gurlo, Interplay between O2 and SnO2: oxygen ionosorption and spectroscopic evidence for adsorbed oxygen, ChemPhysChem 7 (2006) 2041–2052.
[15] M. Anpo, M. Che, B. Fubini, E. Garrone, E. Giamello, M.C. Paganini, Generation of superoxide ions at oxide surfaces, Top. Catal. 8 (1999) 189–198.
[16] K. Sobanska, A. Krasowska, T. Mazur, K. Podolska-Serafin, P. Pietrzyk, Z. Sojka, Diagnostic features of EPR spectra of superoxide intermediates on catalytic surfaces and molecular interpretation of their g and A tensors, Top. Catal. 58 (2015) 796–810.
[17] M. Chiesa, E. Giamello, M. Che, EPR characterization and reactivity of surface-localized inorganic radicals and radical ions, Chem. Rev. 110 (3) (2010) 1320–1347, https://doi.org/10.1021/cr800366v.
[18] F. Zasada, W. Piskorz, J. Janas, J. Grybos, P. Indyka, Z. Sojka, Reactive oxygen species on the (100) facet of cobalt spinel nanocatalyst and their relevance in 16O2/18O2 isotopic exchange, deN2O, and deCH4 processes-a theoretical and experimental account, ACS Catal. 5 (2015) 6879–6892.
[19] K. Dyrek, M. Che, EPR as a tool to investigate the transition metal chemistry on oxide surfaces, Chem. Rev. (Washington, D. C.) 97 (1997) 305–331.
[20] M. Che, Z. Sojka, Electron transfer processes at the surface of MoOx/SiO2 catalysts, Top. Catal. 15 (2001) 211–217.
[21] F. Zasada, J. Janas, W. Piskorz, Z. Sojka, Surface oxygen dynamics and H2 oxidation on cobalt spinel surface probed by 18O/16O isotopic exchange and accounted for by DFT molecular modeling: facile interfacial oxygen atoms flipping through transient peroxy intermediate, Res. Chem. Intermed. 43 (2017) 2865–2880.
[22] W. Piskorz, F. Zasada, P. Stelmachowski, A. Kotarba, Z. Sojka, DFT modeling of reaction mechanism and ab initio microkinetics of catalytic N2O decomposition over alkaline earth oxides: from molecular orbital picture account to simulation of transient and stationary rate profiles, J. Phys. Chem. C 117 (2013) 18488–18501.
[23] M. Che, K. Dyrek, C. Louis, EPR studies on the formation of atomic oxygen(1-) (O-) ions on reduced silica-supported molybdenum catalysts prepared by the grafting method, J. Phys. Chem. 89 (1985) 4526–4530.
[24] Z. Sojka, M. Che, EPR investigation of the activation of N2O on Mo/SiO2 catalysts via electron transfer: from N2O as a ligand to adsorbed O.bul. Ion, J. Phys. Chem. 100 (1996) 14776–14785.
[25] J. Schneider, M. Matsuoka, M. Takeuchi, J. Zhang, Y.u. Horiuchi, M. Anpo, D.W. Bahnemann, Understanding TiO 2 photocatalysis: mechanisms and materials, Chem. Rev. 114 (19) (2014) 9919–9986, https://doi.org/10.1021/cr5001892.
[26] T. Berger, M. Sterrer, O. Diwald, E. Knozinger, Charge trapping and photoadsorption of O2 on dehydroxylated TiO2 nanocrystals–an electron paramagnetic resonance study, ChemPhysChem 6 (2005) 2104–2112.
[27] M. Chiesa, M.C. Paganini, S. Livraghi, E. Giamello, Charge trapping in TiO2 polymorphs as seen by electron paramagnetic resonance spectroscopy, Phys. Chem. Chem. Phys. 15 (2013) 9435–9447.
[28] T. Ito, J.H. Lunsford, Synthesis of ethylene and ethane by partial oxidation of methane over lithium-doped magnesium oxide, Nature (London) 314 (1985) 721–722.
[29] J. Kaczmarczyk, F. Zasada, J. Janas, P. Indyka, W. Piskorz, A. Kotarba, Z. Sojka, Thermodynamic stability, redox properties, and reactivity of Mn3O4, Fe3O4, and Co3O4 model catalysts for N2O decomposition: resolving the origins of steady turnover, ACS Catal. 6 (2016) 1235–1246.
[30] Q. Yi, J. Ji, B. Shen, C. Dong, J. Liu, J. Zhang, M. Xing, Singlet oxygen triggered by superoxide radicals in a molybdenum cocatalytic fenton reaction with enhanced REDOX activity in the environment, Environ. Sci. Technol. 53 (2019) 9725–9733.
[31] Z. Yang, J. Qian, A. Yu, B. Pan, Singlet oxygen mediated iron-based Fenton-like catalysis under nanoconfinement, Proc. Natl. Acad. Sci. U. S. A. 116 (2019) 6659–6664.
[32] K. Sobanska, P. Pietrzyk, Z. Sojka, Generation of reactive oxygen species via electroprotic interaction of H2O2 with ZrO2 gel: ionic sponge effect and pH-switchable peroxidase- and catalase-like activity, ACS Catal. 7 (2017) 2935–2947.
[33] C. Gionco, M.C. Paganini, E. Giamello, R. Burgess, C. Di Valentin, G. Pacchioni, Paramagnetic defects in polycrystalline zirconia: an EPR and DFT study, Chem. Mater. 25 (2013) 2243–2253.
[34] F. Zasada, J. Grybos, C. Hudy, J. Janas, Z. Sojka, Total oxidation of lean methane over cobalt spinel nanocubes-Mechanistic vistas gained from DFT modeling and catalytic isotopic investigations, Catal. Today, (2019) Ahead of Print.
[35] E.V. Starokon, S.E. Malykhin, M.V. Parfenov, G.M. Zhidomirov, A.S. Kharitonov, Oxidation of lower alkenes by α-oxygen (FeIII-O.bul.-)α on the FeZSM-5 surface: the epoxidation or the allylic oxidation?, Mol. Catal. 443 (2017) 43–51.
[36] M. Anpo, N. Aikawa, Y. Kubokawa, M. Che, C. Louis, E. Giamello, Photoformation and structure of oxygen anion radicals (O2-) and nitrogen-containing anion radicals adsorbed on highly dispersed titanium oxide anchored onto porous Vycor glass, J. Phys. Chem. 89 (1985) 5689–5694.
[37] A. Kubacka, M. Fernandez-Garcia, G. Colon, Advanced Nanoarchitectures for Solar Photocatalytic Applications, Chem. Rev. (Washington, DC, U. S.), 112 (2012) 1555-1614.
[38] F. Neese, Spin-Hamiltonian parameters from first principle calculations: theory and application, Biol. Magn. Reson. 28 (2009) 175–229.
[39] J.R. Brailsford, J.R. Morton, L.E. Vannotti, Paramagnetic resonance spectra of O- trapped in alkali iodide crystals, J. Chem. Phys. 49 (1968) 2237–2240.
[40] M. Chiesa, M.C. Paganini, E. Giamello, D.M. Murphy, C. Di Valentin, G. Pacchioni, Excess electrons stabilized on ionic oxide surfaces, Acc. Chem. Res. 39 (2006) 861–867.
[41] G. Pinarello, C. Pisani, A. D'Ercole, M. Chiesa, M.C. Paganini, E. Giamello, O. Diwald, O- radical ions on MgO as a tool to unravel structure and location of ionic vacancies at the surface of oxides: a coupled experimental and theoretical investigation, Surf. Sci. 494 (2001) 95–110.
[42] M. Chiesa, M.C. Paganini, E. Giamello, D.M. Murphy, O- radical ions on MgO: a tool for a structural description of the surface, Res. Chem. Intermed. 28 (2002) 205–214.
[43] C. Di Valentin, D. Ricci, G. Pacchioni, M. Chiesa, M.C. Paganini, E. Giamello, O- radical anions on polycrystalline MgO, Surf. Sci. 521 (2002) 104–116.
[44] M. Sterrer, T. Berger, O. Diwald, E. Knoezinger, Energy transfer on the MgO surface, monitored by UV-induced H2 chemisorption, J. Am. Chem. Soc. 125 (2003) 195–199.
[45] M. Sterrer, O. Diwald, E. Knoezinger, P.V. Sushko, A.L. Shluger, Energies and dynamics of photoinduced electron and hole processes on MgO powders, J. Phys. Chem. B 106 (2002) 12478–12482.
[46] M. Chiesa, E. Giamello, C. Di Valentin, G. Pacchioni, The 17O hyperfine structure of trapped holes photo generated at the surface of polycrystalline MgO, Chem. Phys. Lett. 403 (2005) 124–128.
[47] N.-B. Wong, J.H. Lunsford, EPR study of 17O- on magnesium oxide, J. Chem. Phys. 55 (1971) 3007–3012.
[48] S.E. Malykhin, A.M. Volodin, A.F. Bedilo, G.M. Zhidomirov, Generation of O- radical anions on MgO surface: long-distance charge separation or homolytic dissociation of chemisorbed water?, J. Phys. Chem. C 113 (2009) 10350–10353.
[49] R.F. Howe, M. Gratzel, EPR observation of trapped electrons in colloidal titanium dioxide, J. Phys. Chem. 89 (1985) 4495–4499.
[50] O.I. Micic, Y. Zhang, K.R. Cromack, A.D. Trifunac, M.C. Thurnauer, Trapped holes on titania colloids studied by electron paramagnetic resonance, J. Phys. Chem. 97 (1993) 7277–7283.
[51] E.G. Panarelli, S. Livraghi, S. Maurelli, V. Polliotto, M. Chiesa, E. Giamello, Role of surface water molecules in stabilizing trapped hole centres in titanium dioxide (anatase) as monitored by electron paramagnetic resonance, J. Photochem. Photobiol., A 322–323 (2016) 27–34.

[52] M.C. Paganini, M. Chiesa, F. Dolci, P. Martino, E. Giamello, EPR study of the surface basicity of calcium oxide. 3. Surface reactivity and nonstoichiometry, J. Phys. Chem. B 110 (2006) 11918–11923.
[53] M. Sterrer, T. Berger, O. Diwald, E. Knoezinger, A. Allouche, Ozonide ions on the surface of MgO nanocrystals, Top. Catal. 46 (2007) 111–119.
[54] W. Kanzig, M.H. Cohen, Paramagnetic resonance of oxygen in alkali halides, Phys. Rev. Lett. 3 (1959) 509–510.
[55] V. Polliotto, E. Albanese, S. Livraghi, P. Indyka, Z. Sojka, G. Pacchioni, E. Giamello, Fifty-Fifty Zr-Ti solid solution with a TiO2-type structure: electronic structure and photochemical properties of zirconium titanate ZrTiO4, J. Phys. Chem. C 121 (2017) 5487–5497.
[56] E. Giamello, D. Murphy, E. Garrone, A. Zecchina, Formation of superoxide ions upon oxygen adsorption on magnesium-doped magnesium oxide: an EPR investigation, Spectrochim. Acta, Part A 49A (1993) 1323–1330.
[57] M.C. Paganini, M. Chiesa, E. Giamello, S. Coluccia, G. Martra, D.M. Murphy, G. Pacchioni, Color centers at the surface of alkali-earth oxides. A new hypothesis on the location of surface electron traps, Surf. Sci. 421 (1999) 246–262.
[58] M. Chiesa, E. Giamello, C. Di Valentin, G. Pacchioni, Z. Sojka, S. Van Doorslaer, Nature of the chemical bond between metal atoms and oxide surfaces: new evidences from spin density studies of K atoms on alkaline earth oxides, J. Am. Chem. Soc. 127 (2005) 16935–16944.
[59] M. Chiesa, M.C. Paganini, E. Giamello, D.M. Murphy, Partial ionization of cesium atoms at point defects over polycrystalline magnesium oxide, J. Phys. Chem. B 105 (2001) 10457–10460.
[60] E. Giamello, E. Garrone, P. Ugliengo, M. Che, A.J. Tench, Experimental evidence for the hyperfine interaction between a surface superoxide species on magnesium oxide and a neighboring hydroxylic proton, J. Chem. Soc., Faraday Trans. 1 (85) (1989) 3987–3994.
[61] F. Napoli, M. Chiesa, E. Giamello, G. Preda, C. Di Valentin, G. Pacchioni, Formation of superoxo species by interaction of O2 with Na atoms deposited on MgO powders: a combined continuous-wave EPR (CW-EPR), hyperfine sublevel correlation (HYSCORE) and DFT study, Chem. - Eur. J. 16 (2010) 6776–6785.
[62] A.J. Tench, P. Holroyd, Identification of molecular oxygen negative ion adsorbed on magnesium oxide, Chem. Commun. 471–473 (1968).
[63] M. Chiesa, E. Giamello, M.C. Paganini, Z. Sojka, D.M. Murphy, Continuous wave electron paramagnetic resonance investigation of the hyperfine structure of 17O2- adsorbed on the MgO surface, J. Chem. Phys. 116 (2002) 4266–4274.
[64] M. Che, A.J. Tench, Nonequivalency of oxygen nuclei in 17O–2 adsorbed on oxides, Chem. Phys. Lett. 18 (1973) 199–202.
[65] E. Richards, D.M. Murphy, M. Che, An EPR characterisation of stable and transient reactive oxygen species formed under radiative and non-radiative conditions, Res. Chem. Intermed. 45 (2019) 5763–5779.
[66] E. Giamello, Z. Sojka, M. Che, A. Zecchina, Spectroscopic study of superoxide species formed by low-temperature adsorption of oxygen onto cobalt oxide (CoO)-magnesium oxide solid solutions: an example of synthetic heterogeneous oxygen carriers, J. Phys. Chem. 90 (1986) 6084–6091.
[67] Z. Sojka, E. Giamello, M. Che, A. Zecchina, K. Dyrek, Electronic structure and orientation of dioxygen species on the surface of cobalt monoxide-magnesium oxide solid solutions, J. Phys. Chem. 92 (1988) 1541–1547.
[68] P. Pietrzyk, K. Podolska, T. Mazur, Z. Sojka, Heterogeneous binding of dioxygen: EPR and DFT evidence for side-on nickel(II)-superoxo adduct with unprecedented magnetic structure hosted in MFI zeolite, J. Am. Chem. Soc. 133 (2011) 19931–19943.
[69] N. Siedl, P. Guegel, O. Diwald, First combined electron paramagnetic resonance and FT-IR spectroscopic evidence for reversible O2 adsorption on In2O3-x nanoparticles, J. Phys. Chem. C 117 (2013) 20722–20729.
[70] V. Polliotto, S. Livraghi, S. Agnoli, G. Granozzi, E. Giamello, Reversible adsorption of oxygen as superoxide ion on cerium doped zirconium titanate, Appl. Catal., A 580 (2019) 140–148.
[71] S. Livraghi, M.C. Paganini, E. Giamello, G. Di Liberto, S. Tosoni, G. Pacchioni, Formation of reversible adducts by adsorption of oxygen on Ce-ZrO2: an unusual η2 ionic superoxide, J. Phys. Chem. C 123 (2019) 27088–27096.
[72] C. Gionco, E. Giamello, L. Mino, M.C. Paganini, The interaction of oxygen with the surface of CeO2-TiO2 mixed systems: an example of fully reversible surface-to-molecule electron transfer, Phys. Chem. Chem. Phys. 16 (2014) 21438–21445.
[73] J. Yu, J. Chen, C. Li, X. Wang, B. Zhang, H. Ding, ESR signal of superoxide radical anion adsorbed on TiO2 generated at room temperature, J. Phys. Chem. B 108 (2004) 2781–2783.
[74] E. Carter, A.F. Carley, D.M. Murphy, Evidence for O2- radical stabilization at surface oxygen vacancies on polycrystalline TiO2, J. Phys. Chem. C 111 (2007) 10630–10638.
[75] J. Green, E. Carter, D.M. Murphy, Interaction of molecular oxygen with oxygen vacancies on reduced TiO2: site specific blocking by probe molecules, Chem. Phys. Lett. 477 (2009) 340–344.
[76] E. Giamello, M. Volante, B. Fubini, F. Geobaldo, C. Morterra, An EPR study on the formation of the superoxide radical ion on monoclinic zirconia, Mater. Chem. Phys. 29 (1991) 379–386.
[77] T. Bak, M. Rekas, J. Nowotny, C.C. Sorrell, A. Adamski, K. Dyrek, Z. Sojka, Interactions of oxygen with yttria-stabilized zirconia at room temperature, Ionics 7 (2001) 332–338.
[78] A.F. Bedilo, M.A. Plotnikov, N.V. Mezentseva, A.M. Volodin, G.M. Zhidomirov, I.M. Rybkin, K.J. Klabunde, Superoxide radical anions on the surface of zirconia and sulfated zirconia: formation mechanisms, properties and structure, Phys. Chem. Chem. Phys. 7 (2005) 3059–3069.
[79] J. Soria, A. Martinez-Arias, J.C. Conesa, Spectroscopic study of oxygen adsorption as a method to study surface defects on CeO2, J. Chem. Soc., Faraday Trans. 91 (1995) 1669–1678.
[80] A. Martinez-Arias, J.C. Conesa, J. Soria, O2-probe EPR as a method for characterization of surface oxygen vacancies in ceria-based catalysts, Res. Chem. Intermed. 33 (2007) 775–791.
[81] A. Martinez-Arias, M. Fernandez-Garcia, C. Belver, J.C. Conesa, J. Soria, EPR study on oxygen handling properties of ceria, zirconia and Zr-Ce (1: 1) mixed oxide samples, Catal. Lett. 65 (2000) 197–204.
[82] K. Hayashi, S. Matsuishi, M. Hirano, H. Hosono, Formation of oxygen radicals in 12CaO·7Al2O3: instability of extraframework oxide ions and uptake of oxygen gas, J. Phys. Chem. B 108 (2004) 8920–8925.
[83] F. Zasada, J. Janas, W. Piskorz, M. Gorczynska, Z. Sojka, Total oxidation of lean methane over cobalt spinel nanocubes controlled by the self-adjusted redox state of the catalyst: experimental and theoretical account for interplay between the Langmuir-Hinshelwood and Mars-Van Krevelen mechanisms, ACS Catal. 7 (2017) 2853–2867.
[84] S. Anke, G. Bendt, I. Sinev, H. Hajiyani, H. Antoni, I. Zegkinoglou, H. Jeon, R. Pentcheva, B. Roldan Cuenya, S. Schulz, M. Muhler, Selective 2-propanol oxidation over unsupported Co3O4 spinel nanoparticles: mechanistic insights into aerobic oxidation of alcohols, ACS Catal. 9 (2019) 5974–5985.
[85] D. Kong, Y. Zheng, M. Kobielusz, Y. Wang, Z. Bai, W. Macyk, X. Wang, J. Tang, Recent advances in visible light-driven water oxidation and reduction in suspension systems, Mater. Today (Oxford, U. K.) 21 (2018) 897–924.
[86] A.M. Volodin, S.E. Malykhin, G.M. Zhidomirov, O- radical anions on oxide catalysts: formation, properties, and reactions, Kinet. Catal. 52 (2011) 605–619.
[87] A.M. Volodin, Kinetic parameters of the reaction of molecular oxygen with anion-radicals O- on the MgO surface, Kinet. Katal. 35 (1994) 776–779.
[88] A.M. Volodin, EPR studies of [O-.O2] complexes on magnesia surface and their stabilization centers, React. Kinet. Catal. Lett. 44 (1991) 171–177.
[89] J.M. Coronado, A. Javier Maira, A. Martinez-Arias, J.C. Conesa, J. Soria, EPR study of the radicals formed upon UV irradiation of ceria-based photocatalysts, J. Photochem. Photobiol., A 150 (2002) 213–221.
[90] A.R. Gonzalez-Elipe, C. Louis, M. Che, Electronic paramagnetic resonance study of the reactivity toward carbon monoxide and oxygen of oxygen anions adsorbed on silica-supported molybdenum catalysts, J. Chem. Soc., Faraday Trans. 1 (78) (1982) 1297–1302.
[91] R. Huzimura, H. Kurisu, T. Okuda, Interaction of carbon monoxide with surface defects of magnesia: a high vacuum ESR study, Surf. Sci. 197 (1988) 444–456.
[92] J. Soria, A. Martinez-Arias, J.M. Coronado, J.C. Conesa, Electron paramagnetic resonance spectroscopy study of the adsorption of O2 and CO on a Pt/CeO2/Al2O3 catalyst, Colloids Surf.A 115 (1996) 215–221.
[93] Z. Hao, L. Fen, G.Q. Lu, J. Liu, L. An, H. Wang, In situ electron paramagnetic resonance (EPR) study of surface oxygen species on Au/ZnO catalyst for low-temperature carbon monoxide oxidation, Appl. Catal., A 213 (2001) 173–177.
[94] M. Che, K. Dyrek, C. Louis, Role of atomic oxygen(1-) ions in charge-transfer reactions at the surface of silica-supported molybdenum catalysts prepared by the grafting method, J. Phys. Chem. 89 (1985) 4531–4535.
[95] T. Tashiro, T. Ito, K. Toi, Reaction of methane with nitrous oxide over magnesium oxide at low temperatures, J. Chem. Soc., Faraday Trans. 86 (1990) 1139–1146.
[96] D.J. Driscoll, K.D. Campbell, J.H. Lunsford, Surface-generated gas-phase radicals: formation, detection, and role in catalysis, Adv. Catal. 35 (1987) 139–186.
[97] T. Ito, J. Wang, C.H. Lin, J.H. Lunsford, Oxidative dimerization of methane over a lithium-promoted magnesium oxide catalyst, J. Am. Chem. Soc. 107 (1985) 5062–5068.
[98] E. Giamello, P. Ugliengo, E. Garrone, Superoxide ions formed on magnesium oxide through the agency of presorbed molecules. 1. Spectroscopic electron spin resonance features, J. Chem. Soc., Faraday Trans. 1 (85) (1989) 1373–1382.
[99] E. Garrone, E. Giamello, M. Ferraris, G. Spoto, Superoxide ions formed on magnesia through the agency of presorbed molecules. 2. Details on the mechanism, J. Chem. Soc., Faraday Trans. 88 (1992) 333–337.
[100] Z. Sojka, M. Che, EPR study of the interaction of O- ions with CH3OH within the coordination sphere of Mo ions grafted on silica: a new approach for the study of the mechanism of catalytic reactions, J. Phys. Chem. 99 (1995) 5418–5430.

[101] Z. Sojka, M. Che, Insight into interfacial coordination chemistry through EPR spectroscopy, Colloids Surf. A 158 (1999) 165–178.
[102] J.F. Montoya, I. Ivanova, R. Dillert, D.W. Bahnemann, P. Salvador, J. Peral, Catalytic role of surface oxygens in TiO2 photooxidation reactions: aqueous benzene photooxidation with Ti18O2 under anaerobic conditions, J. Phys. Chem. Lett. 4 (2013) 1415–1422.
[103] B.H.J. Bielski, D.E. Cabelli, R.L. Arudi, A.B. Ross, Reactivity of perhydroxyl/superoxide radicals in aqueous solution, J. Phys. Chem. Ref. Data 14 (1985) 1041–1100.
[104] K. Qi, F. Zasada, W. Piskorz, P. Indyka, J. Grybos, M. Trochowski, M. Buchalska, M. Kobielusz, W. Macyk, Z. Sojka, Self-sensitized photocatalytic degradation of colorless organic pollutants attached to rutile nanorods-experimental and theoretical DFT+D studies, J. Phys. Chem. C 120 (2016) 5442–5456.
[105] P. Neta, R.E. Huie, A.B. Ross, Rate constants for reactions of peroxyl radicals in fluid solutions, J. Phys. Chem. Ref. Data 19 (1990) 413–513.
[106] T. Hirakawa, Y. Nosaka, Properties of O2.bul.- and OH.bul. formed in TiO2 aqueous suspensions by photocatalytic reaction and the influence of H2O2 and some ions, Langmuir 18 (2002) 3247–3254.
[107] Y. Nosaka, A.Y. Nosaka, Generation and Detection of Reactive Oxygen Species in Photocatalysis, Chem. Rev. (Washington, DC, U. S.), 117 (2017) 11302-11336.
[108] E. Giamello, P. Rumori, F. Geobaldo, B. Fubini, M.C. Paganini, The interaction between hydrogen peroxide and metal oxides. EPR investigations, Appl. Magn. Reson. 10 (1996) 173–192.
[109] L. Bonoldi, C. Busetto, A. Congiu, G. Marra, G. Ranghino, M. Salvalaggio, G. Spano, E. Giamello, An ESR study of titanium-silicalite in presence of H2O2, Spectrochim. Acta, Part A 58A (2002) 1143–1154.
[110] F. Geobaldo, S. Bordiga, A. Zecchina, E. Giamello, G. Leofanti, G. Petrini, DRS UV-visible and EPR spectroscopy of hydroperoxo and superoxo complexes in titanium silicalite, Catal. Lett. 16 (1992) 109–115.
[111] M. Ziolek, Catalytic liquid-phase oxidation in heterogeneous system as green chemistry goal-advantages and disadvantages of MCM-41 used as catalyst, Catal. Today 90 (2004) 145–150.
[112] M. Ziolek, I. Sobczak, P. Decyk, K. Sobanska, P. Pietrzyk, Z. Sojka, Search for reactive intermediates in catalytic oxidation with hydrogen peroxide over amorphous niobium(V) and tantalum(V) oxides, Appl. Catal., B 164 (2015) 288–296.
[113] X.C. Song, Z.A. Yang, Y.F. Zheng, H.Y. Yin, Catalytic degradation of phenol by Co3O4 nanocubes, Curr. Nanosci. 9 (2013) 128–131.
[114] M. Anpo, Curr. Opin. Solid State Mater. Sci. 7 (2003) 425.
[115] M. Anpo, Photoluminescence spectroscopy, in: G. Ertl, H. Knoezinger, J. Weitkamp (Eds.) Handbook of Heterogeneous Catalysis, Wiley-VCH, 1997, pp. 664.
[116] M. Anpo, Y. Yamada, Y. Kubokawa, S. Coluccia, A. Zecchina, M. Che, Photoluminescence properties of magnesium oxide powders with coordinatively unsaturated surface ions, J. Chem. Soc., Faraday Trans. 1 (84) (1988) 751–764.
[117] S. Higashimoto, G. Costentin, B. Morin, M. Che, An EPR study of physi- and chemisorption of NO on MgO: effect of outgassing temperature and nature of surface sites, Appl. Catal., B 84 (2008) 58–64.
[118] C. Chizallet, G. Costentin, M. Che, F. Delbecq, P. Sautet, Revisiting acido-basicity of the MgO surface by periodic density functional theory calculations: role of surface topology and ion coordination on water dissociation, J. Phys. Chem. B 110 (2006) 15878–15886.
[119] M.-L. Bailly, G. Costentin, J.M. Krafft, M. Che, Discrimination of MgO ions by means of an improved in situ photoluminescence cell and of propyne as probe molecule, Catal. Lett. 92 (2004) 101–105.
[120] M.-L. Bailly, G. Costentin, H. Lauron-Pernot, J.M. Krafft, M. Che, Physicochemical and in situ photoluminescence study of the reversible transformation of oxide ions of low coordination into hydroxyl groups upon interaction of water and methanol with MgO, J. Phys. Chem. B 109 (2005) 2404–2413.
[121] H. Petitjean, J.-M. Krafft, M. Che, H. Lauron-Pernot, G. Costentin, Identification and distribution of surface ions in low coordination of CaO powders with photoluminescence spectroscopy, J. Phys. Chem. C 115 (2011) 751–756.
[122] C. Chizallet, G. Costentin, J.-M. Krafft, H. Lauron-Pernot, M. Che, Kinetic model of energy transfer processes between low-coordinated ions on MgO by photoluminescence decay measurements, ChemPhysChem 7 (2006) 904–911.
[123] C. Chizallet, G. Costentin, H. Lauron-Pernot, J.-M. Krafft, M. Che, F. Delbecq, P. Sautet, Assignment of photoluminescence spectra of MgO powders: TD-DFT cluster calculations combined to experiments. Part I: structure effects on dehydroxylated surfaces, J. Phys. Chem. C 112 (2008) 16629–16637.
[124] M. Anpo, M. Tomonari, M.A. Fox, In situ photoluminescence of titania as a probe of photocatalytic reactions, J. Phys. Chem. 93 (1989) 7300–7302.
[125] M. Anpo, K. Chiba, M. Tomonari, S. Coluccia, M. Che, M.A. Fox, Photocatalysis on native and platinum-loaded titanium dioxide and zinc oxide catalysts. Origin of different reactivities on wet and dry metal oxides, Bull. Chem. Soc. Jpn. 64 (1991) 543–551.
[126] A. Furube, T. Asahi, H. Masuhara, H. Yamashita, M. Anpo, Charge Carrier dynamics of standard TiO2 catalysts revealed by femtosecond diffuse reflectance spectroscopy, J. Phys. Chem. B 103 (1999) 3120–3127.
[127] H. Yamashita, Y. Ichihashi, M. Anpo, M. Hashimoto, C. Louis, M. Che, Photocatalytic decomposition of NO at 275 K on titanium oxides included within Y-zeolites cavities: the structure and role of the active sites, J. Phys. Chem. 100 (1996) 16041–16044.
[128] M. Anpo, J.M. Thomas, Single-site photocatalytic solids for the decomposition of undesirable molecules, Chem. Commun. (Cambridge, U. K.), (2006) 3273-3278.
[129] M. Anpo, Y. Shioya, H. Yamashita, E. Giamello, C. Morterra, M. Che, H.H. Patterson, S. Webber, S. Ouellette, et al., Preparation and Characterization of the Cu+/ZSM-5 Catalyst and Its Reaction with NO under UV Irradiation at 275 K. In situ Photoluminescence, EPR, and FT-IR Investigations, J. Phys. Chem., 98 (1994) 5744-5750.
[130] H. Yamashita, M. Matsuoka, K. Tsuji, Y. Shioya, M. Anpo, M. Che, In-Situ XAFS, photoluminescence, and IR investigations of copper ions included within various kinds of zeolites. Structure of Cu(I) ions and their interaction with CO molecules, J. Phys. Chem. 100 (1996) 397–402.
[131] M. Matsuoka, W.-S. Ju, K. Takahashi, H. Yamashita, M. Anpo, Photocatalytic decomposition of N2O into N2 and O2 at 298 K on Cu(I) ion catalysts anchored onto various oxides. The effect of the coordination state of the Cu(I) ions on the photocatalytic reactivity, J. Phys. Chem. B 104 (2000) 4911–4915.
[132] M. Anpo, Y. Kubokawa, Photoinduced and photocatalytic reactions on supported metal oxide catalysts. Excited states of oxides and reaction intermediates, Rev. Chem. Intermed. 8 (1987) 105–124.
[133] M. Anpo, I. Tanahashi, Y. Kubokawa, Photoluminescence and photoreduction of vanadium pentoxide supported on porous Vycor glass, J. Phys. Chem. 84 (1980) 3440–3443.
[134] S. Dzwigaj, M. Matsuoka, M. Anpo, M. Che, A comparative study of V species in β zeolite by photoluminescence, diffuse reflectance UV-Visible and 51V NMR spectroscopies, Catal. Lett. 72 (2001) 211–214.
[135] S. Dzwigaj, M. Matsuoka, M. Anpo, M. Che, Evidence of three kinds of tetrahedral vanadium (V) species in VSiβ zeolite by diffuse reflectance UV-visible and photoluminescence spectroscopies, J. Phys. Chem. B 104 (2000) 6012–6020.
[136] E. Giamello, D. Murphy, G. Magnacca, C. Morterra, Y. Shioya, T. Nomura, M. Anpo, The interaction of nitric oxide with copper ions in ZSM5: an EPR and IR investigation, J. Catal. 136 (1992) 510–520.
[137] Y. Horiuchi, T. Toyao, M. Takeuchi, M. Matsuoka, M. Anpo, Recent advances in visible-light-responsive photocatalysts for hydrogen production and solar energy conversion - from semiconducting TiO2 to MOF/PCP photocatalysts, Phys. Chem. Chem. Phys. 15 (2013) 13243–13253.
[138] K. Mori, M. Kawashima, M. Che, H. Yamashita, Enhancement of the Photoinduced Oxidation Activity of a Ruthenium(II) Complex Anchored on Silica-Coated Silver Nanoparticles by Localized Surface Plasmon Resonance, Angew. Chem., Int. Ed., 49 (2010) 8598-8601, S8598/8591-S8598/8594.
[139] K. Tanabe, W.F. Holderich, Industrial application of solid acid-base catalysts, Appl. Catal., A 181 (1999) 399–434.
[140] H. Pines, W.M. Stalick, Base-Catalyzed Reactions of Hydrocarbons and Related Compounds, Academic, 1977.
[141] J.M. Fraile, J.I. Garcia, J.A. Mayoral, Basic solids in the oxidation of organic compounds, Catal. Today 57 (2000) 3–16.
[142] H. Hattori, Solid base catalysts: generation of basic sites and application to organic synthesis, Appl. Catal., A 222 (2001) 247–259.
[143] Y. Ono, Solid base catalysts for the synthesis of fine chemicals, J. Catal. 216 (2003) 406–415.
[144] A. Corma, S. Iborra, Optimization of alkaline earth metal oxide and hydroxide catalysts for base-catalyzed reactions, Adv. Catal. 49 (2006) 239–302.
[145] S.H.Y.S. Abdullah, N.H.M. Hanapi, A. Azid, R. Umar, H. Juahir, H. Khatoon, A. Endut, A review of biomass-derived heterogeneous catalyst for a sustainable biodiesel production, Renew. Sustainable Energy Rev. 70 (2017) 1040–1051.
[146] F. Figueras, M.L. Kantam, B.M. Choudary, Solid base catalysts in organic synthesis, Curr. Org. Chem. 10 (2006) 1627–1637.
[147] G. Zhang, X. Zhang, Y. Meng, G. Pan, Z. Ni, S. Xia, Layered double hydroxides-based photocatalysts and visible-light driven photodegradation of organic pollutants: a review, Chem. Eng. J. 392 (2020) 123684.
[148] A.R. Richard, M. Fan, Properties and applications to methanol synthesis catalysis via hydrogenation of carbon oxides, J. Rare Earths 36 (2018) 1127–1135.
[149] N.A.K. Aramouni, J.G. Touma, B. Abu Tarboush, J. Zeaiter, M.N. Ahmad, Catalyst design for dry reforming of methane: Analysis review, Renew. Sustainable Energy Rev. 82 (2018) 2570–2585.
[150] Y. Gambo, A.A. Jalil, S. Triwahyono, A.A. Abdulrasheed, Recent advances and future prospect in catalysts for oxidative coupling of methane to ethylene: A review, J. Ind. Eng. Chem. (Amsterdam, Neth.) 59 (2018) 218–229.
[151] K.-I. Shimizu, Heterogeneous catalysis for the direct synthesis of chemicals by borrowing hydrogen methodology, Catal. Sci. Technol. 5 (2015) 1412–1427.
[152] J.T. Kozlowski, R.J. Davis, Heterogeneous catalysts for the guerbet coupling of alcohols, ACS Catal. 3 (2013) 1588–1600.
[153] J.N. Bronsted, The conception of acids and bases, Recl. Trav. Chim. Pays-Bas Belg. 42 (1923) 718–728.

[154] U. Meyer, W.F. Hoelderich, Application of basic zeolites in the decomposition reaction of 2-methyl-3-butyn-2-ol and the isomerization of 3-carene, J. Mol. Catal. A: Chem. 142 (1999) 213–222.
[155] J.C. Lavalley, Infrared spectrometric studies of the surface basicity of metal oxides and zeolites using adsorbed probe molecules, Catal. Today 27 (1996) 377–401.
[156] V.K. Diez, C.R. Apesteguia, J.I. Di Cosimo, Acid-base properties and active site requirements for elimination reactions on alkali-promoted MgO catalysts, Catal. Today 63 (2000) 53–62.
[157] G. Pacchioni, J.M. Ricart, F. Illas, Ab initio cluster model calculations on the chemisorption of CO2 and SO2 probe molecules on MgO and CaO (100) surfaces. A theoretical measure of oxide basicity, J. Am. Chem. Soc. 116 (1994) 10152–10158.
[158] C. Angelici, M.E.Z. Velthoen, B.M. Weckhuysen, P.C.A. Bruijnincx, Influence of acid-base properties on the Lebedev ethanol-to-butadiene process catalyzed by SiO2-MgO materials, Catal. Sci. Technol. 5 (2015) 2869–2879.
[159] H. Lauron-Pernot, F. Luck, J.M. Popa, Methylbutynol: a new and simple diagnostic tool for acidic and basic sites of solids, Appl. Catal. 78 (1991) 213–225.
[160] M.-L. Bailly, C. Chizallet, G. Costentin, J.-M. Krafft, H. Lauron-Pernot, M. Che, A spectroscopy and catalysis study of the nature of active sites of MgO catalysts: thermodynamic Bronsted basicity versus reactivity of basic sites, J. Catal. 235 (2005) 413–422.
[161] D. Cornu, H. Guesmi, J.-M. Krafft, H. Lauron-Pernot, Lewis acido-basic interactions between CO2 and MgO surface: DFT and DRIFT approaches, J. Phys. Chem. C 116 (2012) 6645–6654.
[162] C. Chizallet, G. Costentin, M. Che, F. Delbecq, P. Sautet, Infrared characterization of hydroxyl groups on MgO: a periodic and cluster density functional theory study, J. Am. Chem. Soc. 129 (2007) 6442–6452.
[163] C. Chizallet, G. Costentin, H. Lauron-Pernot, J.-M. Krafft, M. Che, F. Delbecq, P. Sautet, Assignment of photoluminescence spectra of MgO powders: TD-DFT cluster calculations combined to experiments. Part II. Hydroxylation effects, J. Phys. Chem. C 112 (2008) 19710–19717.
[164] E. Knoezinger, K.-H. Jacob, S. Singh, P. Hofmann, Hydroxyl groups as IR active surface probes on MgO crystallites, Surf. Sci. 290 (1993) 388–402.
[165] C. Chizallet, G. Costentin, H. Lauron-Pernot, M. Che, C. Bonhomme, J. Maquet, F. Delbecq, P. Sautet, Study of the structure of OH groups on MgO by 1D and 2D 1H MAS NMR combined with DFT cluster calculations, J. Phys. Chem. C 111 (2007) 18279–18287.
[166] C. Chizallet, G. Costentin, H. Lauron-Pernot, J. Maquet, M. Che, 1H MAS NMR study of the coordination of hydroxyl groups generated upon adsorption of H2O and CD3OH on clean MgO surfaces, Appl. Catal., A 307 (2006) 239–244.
[167] C. Chizallet, M.L. Bailly, G. Costentin, H. Lauron-Pernot, J.M. Krafft, P. Bazin, J. Saussey, M. Che, Thermodynamic Bronsted basicity of clean MgO surfaces determined by their deprotonation ability: role of Mg2+-O2- pairs, Catal. Today 116 (2006) 196–205.
[168] C. Chizallet, H. Petitjean, G. Costentin, H. Lauron-Pernot, J. Maquet, C. Bonhomme, M. Che, Identification of the OH groups responsible for kinetic basicity on MgO surfaces by 1H MAS NMR, J. Catal. 268 (2009) 175–179.
[169] H. Petitjean, H. Guesmi, H. Lauron-Pernot, G. Costentin, D. Loffreda, P. Sautet, F. Delbecq, How surface hydroxyls enhance MgO reactivity in basic catalysis: the case of methylbutynol conversion, ACS Catal. 4 (2014) 4004–4014.
[170] H. Petitjean, C. Chizallet, J.-M. Krafft, M. Che, H. Lauron-Pernot, G. Costentin, Basic reactivity of CaO: investigating active sites under operating conditions, Phys. Chem. Chem. Phys. 12 (2010) 14740–14748.
[171] C.R. Ho, S. Zheng, S. Shylesh, A.T. Bell, The mechanism and kinetics of methyl isobutyl ketone synthesis from acetone over ion-exchanged hydroxyapatite, J. Catal. 365 (2018) 174–183.
[172] P. Valvekens, M. Vandichel, M. Waroquier, V. Van Speybroeck, D. De Vos, Metal-dioxidoterephthalate MOFs of the MOF-74 type: Microporous basic catalysts with well-defined active sites, J. Catal. 317 (2014) 1–10.
[173] D. Cornu, H. Petitjean, G. Costentin, H. Guesmi, J.-M. Krafft, H. Lauron-Pernot, Influence of natural adsorbates of magnesium oxide on its reactivity in basic catalysis, Phys. Chem. Chem. Phys. 15 (2013) 19870–19878.
[174] G.A. Mutch, S. Shulda, A.J. McCue, M.J. Menart, C.V. Ciobanu, C. Ngo, J.A. Anderson, R.M. Richards, D. Vega-Maza, Carbon capture by metal oxides: unleashing the potential of the (111) facet, J. Am. Chem. Soc. 140 (2018) 4736–4742.
[175] G. Pomalaza, P. Arango Ponton, M. Capron, F. Dumeignil, Ethanol-to-butadiene: the reaction and its catalysts, Catal. Sci. Technol. 10 (2020) 4860–4911.
[176] M. Zhang, F. Averseng, J.-M. Krafft, P. Borghetti, G. Costentin, S. Stankic, Controlled formation of native defects in ultrapure ZnO for the assignment of green emissions to oxygen vacancies, J. Phys. Chem. C 124 (2020) 12696–12704.
[177] M. Zhang, F. Averseng, F. Haque, P. Borghetti, J.-M. Krafft, B. Baptiste, G. Costentin, S. Stankic, Defect-related multicolour emissions in ZnO smoke: from violet, over green to yellow, Nanoscale 11 (2019) 5102–5115.
[178] C. Drouilly, J.-M. Krafft, F. Averseng, S. Casale, D. Bazer-Bachi, C. Chizallet, V. Lecocq, H. Vezin, H. Lauron-Pernot, G. Costentin, ZnO oxygen vacancies formation and filling followed by in situ photoluminescence and in situ EPR, J. Phys. Chem. C 116 (2012) 21297–21307.
[179] C. Drouilly, J.-M. Krafft, F. Averseng, H. Lauron-Pernot, D. Bazer-Bachi, C. Chizallet, V. Lecocq, G. Costentin, Role of oxygen vacancies in the basicity of ZnO: from the model methylbutynol conversion to the ethanol transformation application, Appl. Catal., A 453 (2013) 121–129.
[180] C. Drouilly, J.-M. Krafft, F. Averseng, H. Lauron-Pernot, D. Bazer-Bachi, C. Chizallet, V. Lecocq, G. Costentin, Origins of the deactivation process in the conversion of methylbutynol on zinc oxide monitored by operando DRIFTS, Catal. Today 205 (2013) 67–75.
[181] L.H. Chagas, P.C. Zonetti, C.R.V. Matheus, C.R.K. Rabello, O.C. Alves, L.G. Appel, The role of the oxygen vacancies in the synthesis of 1,3-butadiene from ethanol, ChemCatChem 11 (2019) 5625–5632.
[182] M. Xu, M. Wei, Layered Double Hydroxide-Based Catalysts: Recent Advances in Preparation, Structure, and Applications, Adv. Funct. Mater., 28 (2018) n/a.
[183] F. Winter, X. Xia, B.P.C. Hereijgers, J.H. Bitter, A.J. Van Dillen, M. Muhler, K.P. De Jong, On the nature and accessibility of the bronsted-base sites in activated hydrotalcite catalysts, J. Phys. Chem. B 110 (2006) 9211–9218.
[184] L. Lin, D. Cornu, M. Mounir Daou, C. Domingos, V. Herledan, J.-M. Krafft, G. Laugel, Y. Millot, H. Lauron-Pernot, Role of water on the activity of magnesium silicate for transesterification reactions, ChemCatChem 9 (2017) 2399–2407.
[185] D. Fan, X. Dong, Y. Yu, M. Zhang, A DFT study on the aldol condensation reaction on MgO in the process of ethanol to 1,3-butadiene: understanding the structure-activity relationship, Phys. Chem. Chem. Phys. 19 (2017) 25671–25682.
[186] S. Diallo-Garcia, D. Laurencin, J.-M. Krafft, S. Casale, M.E. Smith, H. Lauron-Pernot, G. Costentin, Influence of magnesium substitution on the basic properties of hydroxyapatites, J. Phys. Chem. C 115 (2011) 24317–24327.
[187] S. Petit, T. Gode, C. Thomas, S. Dzwigaj, Y. Millot, D. Brouri, J.-M. Krafft, G. Rousse, C. Laberty-Robert, G. Costentin, Incorporation of vanadium into the framework of hydroxyapatites: importance of the vanadium content and pH conditions during the precipitation step, Phys. Chem. Chem. Phys. 19 (2017) 9630–9640.
[188] S. Petit, C. Thomas, Y. Millot, J.-M. Krafft, C. Laberty-Robert, G. Costentin, Activation of C-H bond of propane by strong basic sites generated by bulk proton conduction on V-modified hydroxyapatites for the formation of propene, ChemCatChem 12 (2020) 2506–2521.
[189] M. Ben Osman, J.M. Krafft, Y. Millot, F. Averseng, T. Yoshioka, J. Kubo, G. Costentin, Molecular understanding of the bulk composition of crystalline nonstoichiometric hydroxyapatites: application to the rationalization of structure-reactivity relationships, Eur. J. Inorg. Chem. (2016, 2016,) 2709–2720.
[190] S. Diallo-Garcia, M. Ben Osman, J.-M. Krafft, S. Boujday, C. Guylene, Discrimination of infrared fingerprints of bulk and surface POH and OH of hydroxyapatites, Catal. Today 226 (2014) 81–88.
[191] M. Ben Osman, S. Diallo-Garcia, V. Herledan, D. Brouri, T. Yoshioka, J. Kubo, Y. Millot, G. Costentin, Discrimination of surface and bulk structure of crystalline hydroxyapatite nanoparticles by NMR, J. Phys. Chem. C 119 (2015) 23008–23020.
[192] S. Diallo-Garcia, M.B. Osman, J.-M. Krafft, S. Casale, C. Thomas, J. Kubo, G. Costentin, Identification of surface basic sites and acid-base pairs of hydroxyapatite, J. Phys. Chem. C 118 (2014) 12744–12757.
[193] M. Ben Osman, S.D. Garcia, J.-M. Krafft, C. Methivier, J. Blanchard, T. Yoshioka, J. Kubo, G. Costentin, Control of calcium accessibility over hydroxyapatite by post-precipitation steps: influence on the catalytic reactivity toward alcohols, Phys. Chem. Chem. Phys. 18 (2016) 27837–27847.
[194] M.B. Osman, J.-M. Krafft, C. Thomas, T. Yoshioka, J. Kubo, G. Costentin, Importance of the nature of the active acid/base pairs of hydroxyapatite involved in the catalytic transformation of ethanol to n-butanol revealed by Operando DRIFTS, ChemCatChem 11 (2019) 1765–1778.
[195] A. Brueckner, E. Kondratenko, Simultaneous operando EPR/UV-vis/laser-Raman spectroscopy - a powerful tool for monitoring transition metal oxide catalysts during reaction, Catal. Today 113 (2006) 16–24.
[196] P. Pietrzyk, Z. Sojka, E. Giamello, Electron paramagnetic resonance spectroscopy, Wiley-VCH Verlag GmbH & Co. KGaA, 2012, pp. 343-406.
[197] E. Morra, E. Giamello, M. Chiesa, EPR approaches to heterogeneous catalysis. The chemistry of titanium in heterogeneous catalysts and photocatalysts, J. Magn. Reson. 280 (2017) 89–102.
[198] E. Morra, M. Signorile, E. Salvadori, S. Bordiga, E. Giamello, M. Chiesa, Nature and topology of metal-oxygen binding sites in zeolite materials: 17O high-resolution EPR spectroscopy of metal-loaded ZSM-5, Angew. Chem., Int. Ed. 58 (2019) 12718.
[199] V. Lagostina, E. Salvadori, M. Chiesa, E. Giamello, Electron paramagnetic resonance study of vanadium exchanged H-ZSM5 prepared by vapor reaction of VCl4. The role of17O isotope labelling inthe characterisation of the metal oxide interaction, J. Catal. 391 (2020) 397–403.

[200] W.E. Taifan, T. Bucko, J. Baltrusaitis, Catalytic conversion of ethanol to 1,3-butadiene on MgO: a comprehensive mechanism elucidation using DFT calculations, J. Catal. 346 (2017) 78–91.
[201] P. Carniti, A. Gervasini, Liquid-Solid Adsorption Properties: Measurement of the Effective Surface Acidity of Solid Catalysts, in: A. Auroux (Ed.), Calorimetry and Thermal Methods in Catalysis, Springer, Berlin Heidelberg, Berlin, Heidelberg, 2013, pp. 543–551.